PRIMER

Force spectroscopy of single cells using atomic force microscopy

Albertus Viljoen[1], *Marion Mathelié-Guinlet*[1], *Ankita Ray*[1], *Nico Strohmeyer*[2], *Yoo Jin Oh*[3], *Peter Hinterdorfer*[3]✉, *Daniel J. Müller*[2]✉, *David Alsteens*[1]✉ *and Yves F. Dufrêne*[1]✉

Abstract | Physical forces and mechanical properties have critical roles in cellular function, physiology and disease. Over the past decade, atomic force microscopy (AFM) techniques have enabled substantial advances in our understanding of the tight relationship between force, mechanics and function in living cells and contributed to the growth of mechanobiology. In this Primer, we provide a comprehensive overview of the use of AFM-based force spectroscopy (AFM-FS) to study the strength and dynamics of cell adhesion from the cellular to the single-molecule level, spatially map cell surface receptors and quantify how cells dynamically regulate their mechanical and adhesive properties. We first introduce the importance of force and mechanics in cell biology and the general principles of AFM-FS methods. We describe procedures for sample and AFM probe preparations, the various AFM-FS modalities currently available and their respective advantages and limitations. We also provide details and recommendations for best usage practices, and discuss data analysis, statistics and reproducibility. We then exemplify the potential of AFM-FS in cellular and molecular biology with a series of recent successful applications focusing on viruses, bacteria, yeasts and mammalian cells. Finally, we speculate on the grand challenges in the area for the next decade.

Energy landscape
A description in two or three dimensions of the energetic and kinetic properties of a specific bond, for example, receptor–ligand bonds

[1]*Louvain Institute of Biomolecular Science and Technology, Université Catholique de Louvain, Louvain-la-Neuve, Belgium.*

[2]*Departement of Biosystems Science and Engineering, ETH Zurich, Basel, Switzerland.*

[3]*Institute of Biophysics, Johannes Kepler University, Linz, Austria.*

✉*e-mail: Peter.Hinterdorfer@jku.at; daniel.mueller@bsse.ethz.ch; David.Alsteens@uclouvain.be; Yves.Dufrene@uclouvain.be*

https://doi.org/10.1038/s43586-021-00062-x

Mechanobiology is a multidisciplinary, fast-growing field aiming at understanding how mechanical forces control cell function, physiology and disease[1–12]. In nature, most biological systems, from viruses to human tissues, are subject to mechanical forces either self-generated or imposed by their environment. A key question therefore centres around the mechanisms developed by living cells to cope with mechanical cues by which they exert, sense and respond to mechanical force. For instance, how does bacterial cell behaviour depend on fluid shear stress, such as in the blood or in the urinary tract, and to what extent does this dependency contribute to host colonization and infection? How do cells, tissues and organs incorporate mechanical cues to orchestrate development and physiology or, in case of non-physiological forces, trigger diseases? To answer these questions, one of the most versatile platforms for probing cellular interactions in both whole cells and single molecules is atomic force microscopy (AFM)-based force spectroscopy (AFM-FS).

Mechanical forces and cell functions

Mechanical forces play essential roles in cellular processes such as adhesion, migration, signalling, sensing and tissue development, as well as diseases such as cancer, fibrosis and bacterial infection[13]. Specific molecular interactions that bear these mechanical forces result from a complex interplay of fundamental hydrophobic, electrostatic, van der Waals and hydrogen bond forces. Knowledge of the biophysical details of these specific molecular interactions such as strength, dynamics, energy landscape and reaction kinetics is thus critical to our understanding of the basic processes of life. Biomolecular forces can range from a few pN that single molecular motors, such as the motor proteins myosin and kinesin[14,15], can exert to 20–250 pN that single proteins[16,17] and most receptor–ligand interactions[18,19] can bear before unfolding and dissociating, respectively. In comparison, the force required to rupture a single covalent bond is in the order of 2–4 nN (REF.[20]). When it comes to whole cells, the cellular adhesion force can range from hundreds of pN to several tens of nN, as up to several hundreds of biomolecular interactions are generally probed in parallel[13]. In contrast to bulk biological methods that probe large ensembles of molecules or cells, AFM can manipulate single cells and single molecules in living and physiologically relevant conditions to enable the discovery of new and unanticipated behaviours, properties and interactions. Furthermore, compared with optical and magnetic tweezers used in molecular biology[21–23], AFM offers the possibility to measure a much

Cellular adhesion force
The force cells withstand before detaching from surfaces, for example, from extracellular matrix (ECM) proteins, other cells or substrates.

Cortical elasticity
The elasticity of the actomyosin cortex of a mammalian cell.

Cantilever deflection
Bending of the cantilever in response to forces applied to the cantilever.

wider range of forces, typically from as low as 5 pN up to >100 nN (REFS[24–27]), and stiffnesses from about 100 Pa to the low GPa range[28,29]. AFM can also simultaneously localize receptors on cells that participate in the probed interactions with a lateral resolution of ~50–100 nm depending on the size of the probed molecules and cellular topography. This is an important asset as biomolecular interactions in living cells are directly linked to the dynamic formation of structures and compartments.

In addition to biological forces, cell elasticity also regulates numerous cellular processes during healthy and disease states. The elasticity of mammalian cells, often expressed in terms of the Young's modulus *E*, can depend on cell shape, membrane tension, the actomyosin cortex or cellular compartments, all of which change dynamically during the cell cycle, in response to mechanical impediments or as the result of biochemical signalling[1,30,31]. For instance, cortical elasticity fulfils a regulatory function during physiological processes such as cell division[32,33] whereas cell mechanical properties can significantly change during cell development and disease such as cancer[34–36]. As opposed to mammalian cells, which are relatively soft (*E* smaller than ~10 kPa), microbial cells such as bacteria or yeasts possess a thick and stiff cell wall (*E* can exceed several MPa)[37–39]. Mammalian and microbial cells often feature local elasticity variations due to the complex, anisotropic composition of their membranes, walls and inner components[40]. As is discussed below, nanoindentation experiments using AFM-FS have become an invaluable approach to measure the local elastic properties of living cells in relation to function while simultaneously imaging their topography.

Principles of AFM

The AFM is a multifunctional tool capable of imaging the topography of biological systems at nanometre resolution under physiological conditions and of quantifying biophysical properties and molecular interactions. The heart of an atomic force microscope consists of a sharp tip, typically ended with a nanometre-sized apex, attached to the free end of a soft cantilever (FIG. 1a). The principle of operation is to monitor the forces acting between the tip and the sample surface. The tip–sample interaction forces cause the cantilever to deflect, which is recorded via a laser beam that is focused on the free end of the cantilever and reflected onto a position-sensitive photodiode. The cantilever deflection, *d*, is directly proportional to the force, *F*, acting between the tip and the sample, through the relationship $F = -k \cdot d$, with *k* being the spring constant of the cantilever. A piezoelectric scanner that moves either the cantilever or the sample allows the tip to scan the sample surface in *x* and *y* directions whereas a feedback loop between the deflection of the cantilever and the *z*-piezo allows control of the precise position of the tip and the applied force.

In topographic imaging, the atomic force microscope raster scans the tip along the sample to contour its three-dimensional topography[41]. Topographical mapping can be achieved using contact mode AFM, where the tip is in permanent contact with the sample and the applied force is kept constant by continually adjusting the vertical distance — the height — of the tip or sample through the feedback loop. In dynamic mode AFM, the tip is oscillated near the sample surface, either in non-contact or intermittent contact, and the oscillation amplitude or frequency is kept constant through the feedback loop. For soft samples such as animal cells, dynamic modes might be advantageous to lower the force acting on the sample and minimize surface damage or image artefacts. Large forces acting between the tip and the sample during imaging may also dramatically reduce the image resolution and cause molecular damage or displacement. In theory, the spatial resolution achieved on flat and smooth surfaces can be ≤1 nm in the horizontal plane and as low as 0.1 nm in the vertical plane[41].

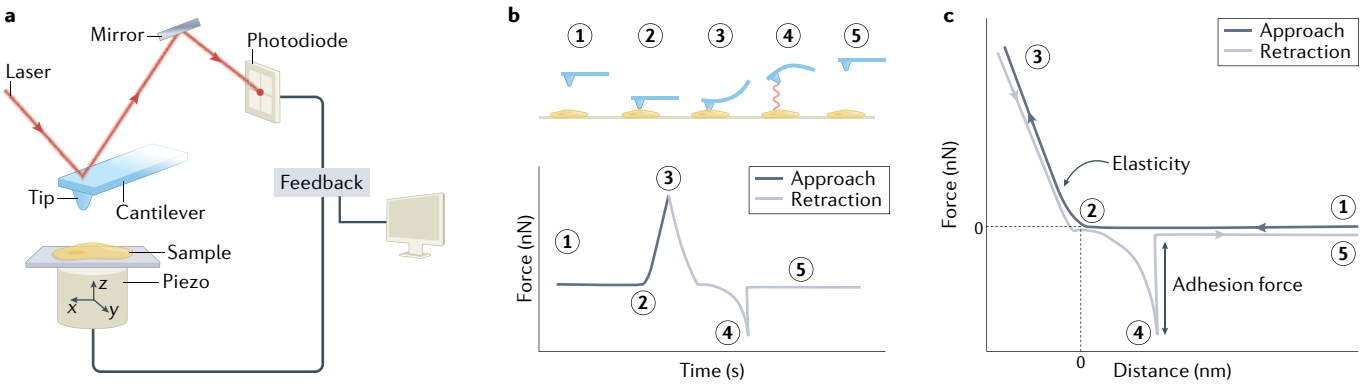

Fig. 1 | **General principles of AFM-FS. a** | In atomic force microscopy (AFM), a sample is probed with a very sharp tip attached to the free end of a flexible cantilever. A laser is focused on the cantilever above the tip and reflected via a mirror onto a photodiode. Forces exerted by the sample on the tip cause deflection of the cantilever and change the path of the laser, which is detected by the photodiode and recorded by a computer. Recorded data can be converted into units of force. A feedback system controls a set of piezos that, in turn, control the *x*–*y*–*z* position of the sample. **b**,**c** | Generation of force versus time (part **b**) and force versus distance (part **c**) curves using AFM-based force spectroscopy (AFM-FS). (1–3) The *z*-piezo brings the tip (blue) and a sample (for example, the cell shown in yellow) into contact (2) and, eventually, repulsive forces exerted by the sample on the tip lead to an upward cantilever deflection registered as a positive force (3). (3–5) Once an arbitrary applied force is registered, the feedback system reverses the motion of the *z*-piezo and the sample is displaced away from the tip. Attractive forces between the tip and sample cause a downward deflection of the cantilever (4). Upon rupture of the tip–sample contact, the cantilever returns to its rest position (5). **c** | Force–distance curves can be analysed to extract the adhesion force and the elasticity of a cell. When the tip is functionalized with bioligands, the strength of single receptor–ligand interactions can be measured.

In this Primer, we focus on the ability of AFM to work as an ultra-sensitive force sensor using the force spectroscopy modality[13]. The basic idea is to acquire force–distance or force–time curves, in which the force applied or experienced by the AFM tip is monitored as a function of the distance between the tip and the sample surface or as a function of time (FIG. 1b,c). As the tip approaches the sample, comes into contact with it, pushes on it and, finally, retracts, the sample's biophysical properties such as elasticity and adhesion can be obtained. Functionalizing the tip or the cantilever with cells, biomolecules or chemical groups enables measurement of single-cell adhesion, and specific biological and chemical interactions.

Major technical advances made in biological AFM-FS started with the invention of AFM in 1986, its implementation to analyse living cells in buffer solution[42–44], the quantification and mapping of molecular forces by recording single force–distance curves[45,46] or force–distance curve arrays (also called force volume[47–49]) and the development of multiparametric AFM, which simultaneously provides images of the sample surface and maps its biophysical properties and molecular interactions at very high resolution[49–54]. Today, platforms correlating AFM-FS with advanced optical microscopy techniques have become very popular as they allow coupling the optical morphology and protein localization of complex biological samples with their mechanical and adhesive properties[55,56].

This Primer focuses on the use of AFM-FS for studying complex biological systems including viruses, bacteria, yeasts, and mammalian cells and tissues. As such, it does not cover AFM-FS experiments on purified biomolecules (for a review see REF.[25]), AFM topographic imaging of cellular systems per se (see REF.[41]) or AFM-FS indentation experiments in great detail (for a recent exhaustive review see REF.[31]). The examples discussed in this Primer were mainly obtained with commercially available AFM hardware and software, but the main principles and approaches (experimental set-up, force–distance curve generation and data analysis) also apply to custom-built hardware. We hope this Primer is useful to AF microscopists but also for newcomers from biophysics, cell biology and microbiology, who generally use ensemble rather than single-cell and single-molecule experimental techniques. We start with an Experimentation section in which we outline the fundamental principles of the main AFM-FS modalities and provide general guidelines to how force spectroscopy experiments are conducted. In the Results section, we discuss how to extract and present relevant parameters for the various modalities, which we follow with an Applications section using examples of successful studies across fields and disciplines. We also discuss statistics and reproducibility, and limitations and optimizations of the method, and speculate on the grand challenges in the area for the next decade.

Experimentation

After explaining how force–distance curves are obtained, we survey the fundamental principles of the main AFM-FS modalities in biology: single-molecule and single-cell force spectroscopy (SMFS and SCFS), multiparametric imaging, force and height clamp, and nanoindentation experiments. We also detail sample preparation procedures and tip (SMFS) or cantilever (SCFS) functionalization, which are key factors for successful experiments.

How to record force–distance curves

A force–distance curve is obtained by monitoring the deflection of the cantilever via the reflection of a laser beam as a function of the vertical displacement of the cantilever through a piezoelectric scanner. Thereby, the cantilever displacement is measured either by calibrated piezoelectric elements or by a capacitive sensor. Further, the set-up records voltage variations on a position-sensitive photodiode caused by movement of the laser in response to the cantilever deflection that are converted into force through determination of both the cantilever sensitivity, s (metres per volt), and the spring constant, k (newtons per metre). The cantilever sensitivity is determined by recording a force–distance curve on a stiff surface such as mica or glass and extracting the slope of the contact portion. The spring constant of the cantilever can be determined by different approaches, including reference cantilever[57,58], resonance frequency and thermal noise methods[59], the latter of which are currently the most frequently used in commercially available systems. As the distance signal in force–distance curves contains piezo displacement and cantilever deflection in the contact region, the piezoelectric scanner displacement needs to be converted into a tip–sample separation distance. This requires the identification of the contact point, which for deformable cells can be delicate. Various automated approaches have been proposed for determination of the contact point[60–65].

Numerous sample properties and interactions can be derived from force–distance curves (FIG. 1c). Upon approach, the tip and the sample surface are first far enough apart not to interact, resulting in null force. Decreasing the tip–sample distance results in diverse long-range and short-range repulsive or attractive interactions (for example, electrostatic or van der Waals forces), until the tip makes contact with the surface. As the tip is further pushed against the sample, it induces an upward deflection of the cantilever. From this contact region, dedicated contact models allow the extraction of the sample elastic properties such as deformation, elasticity and stiffness. When a predefined force is reached, the motion of the tip is halted and reversed. As the tip is moved upward the cantilever relaxes, and then often deflects downward owing to adhesive forces between the tip and sample. This hysteresis between the retract and approach portions of the force–distance curve is important because it provides the adhesion force of the system as the maximum downward deflection of the cantilever during retraction and the adhesion work as the integral of the force over distance. By functionalizing the AFM probe with biomolecules in SMFS or with cells in SCFS, the strength of molecular and cellular interactions, respectively, can be measured. Finally, the tip–surface contact ruptures and the cantilever goes back to its zero force position.

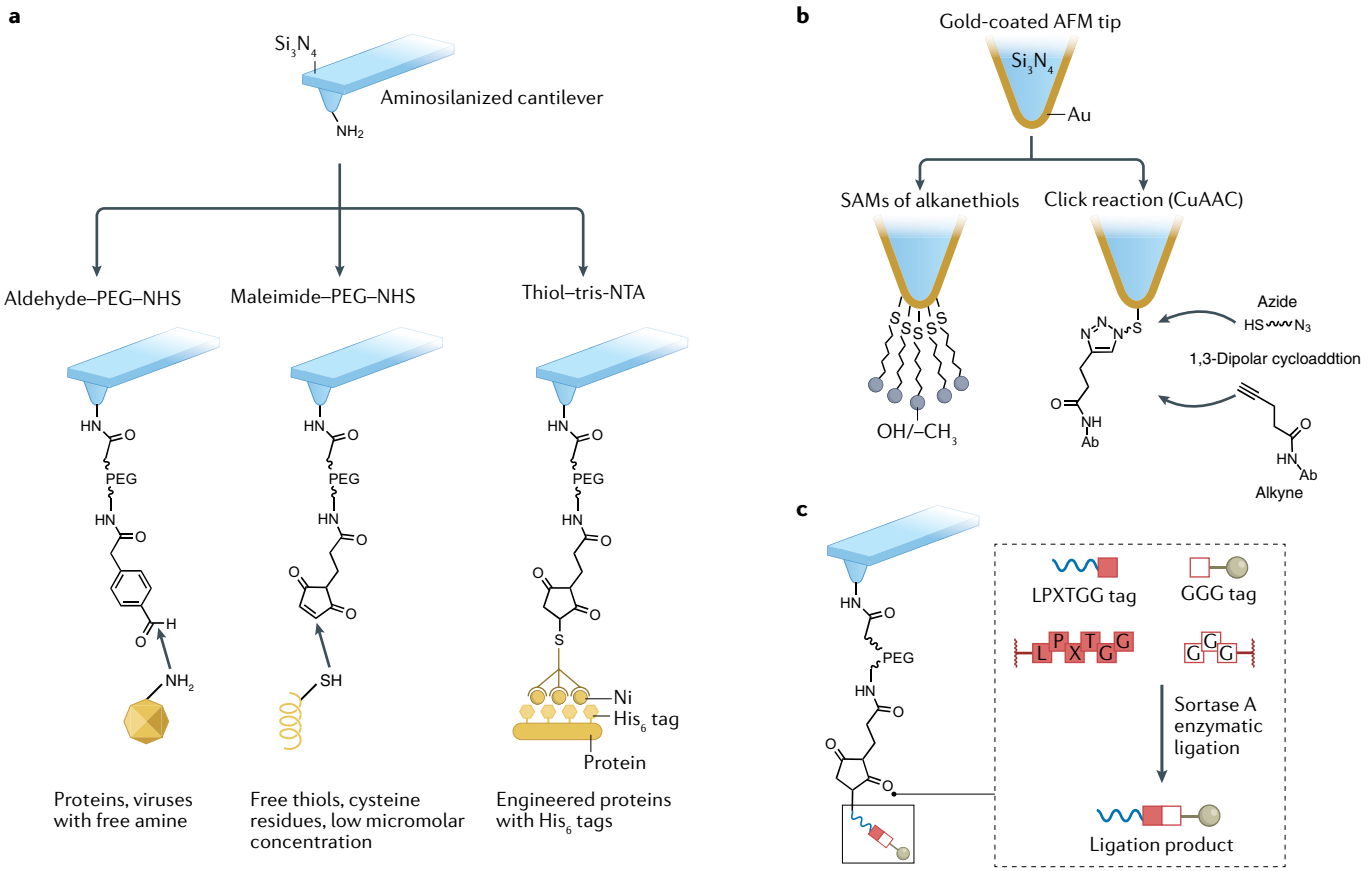

Fig. 2 | **Schematic representation of various surface functionalization strategies to anchor biomolecules on inorganic surfaces for single-molecule force spectroscopy. a** | Overview of aminosilanized atomic force microscopy (AFM) tips covalently modified with biomolecules via different heterobifunctional poly(ethylene glycol) (PEG) linkers. **b** | Surface modification of gold-coated AFM tip by self-assembled monolayer (SAM) formation and click reaction chemistry. **c** | Enzymatic-assisted AFM tip modification using LPXTGG tag/GGGtag/Sortase A. Ab, antibody; CuAAC, copper(I)-assisted azide–alkyne cycloaddition.

Immobilization of cells for AFM-FS

For reliable AFM-FS experiments, microbial or animal cells must be immobilized on an appropriate substrate using non-destructive protocols to resist the forces exerted by the tip[66]. For many cell types, smooth hydrophilic glass and mica are appropriate substrates[56,67–71]. Certain cell types require hydrophobic surfaces to strengthen attachment, such as polystyrene Petri dishes or solid supports coated with hydrophobic polymers. For applications requiring well-defined surface chemistry, self-assembled monolayers of organic alkanethiols on gold are very useful[72,73].

One should avoid drying or fixing cells with chemicals such as glutaraldehyde or paraformaldehyde as this will alter their functionality, physical properties such as elasticity and interactions such as adhesion with their environment. Typically, animal cells naturally tend to spread and adhere to solid supports[44]. Rigid microbial cells, however, generally require stronger immobilization procedures. It is possible to coat the support with polycations, but this can contaminate the AFM tip and make it unsuitable for AFM-FS analyses. A good alternative is to mechanically immobilize the bacteria or yeasts in a porous polymer membrane with a pore size similar to the microbial cell dimensions[74,75]. The method works well for spherical bacterial and yeast cells but typically becomes more complicated for rod-shaped bacteria.

Single-molecule force spectroscopy

Today, SMFS is routinely applied to probe single-molecule interactions on living cells. This requires modifying the AFM tip with cognate ligands to detect and force probe single-molecule interactions[18]. The protocol used should ensure strong attachment of the molecules while retaining their flexibility, low grafting density to guarantee single-molecule detection, a non-sticky background surface to prevent non-specific adsorption and tip contamination, for example, by the cell glycocalyx[56,67–71], and specific orientation of the ligand for some applications.

To this end, a wide repertoire of AFM tip functionalization strategies has been developed[18,76,77] (FIG. 2). Biomolecules can be chemically attached using a short linker whereas the rest of the tip apex is blocked by spacer molecules that help discriminate between specific and non-specific interactions. However, high coverage of ligands increases the risk of probing multiple binding events and increases steric hindrance, which can interfere with the binding process. Hence, the molecule/spacer ratio is usually maintained at about

Cognate ligands
Ligands specifically binding to a receptor.

1:100 or 1:1,000 (REF.[78]) to control the ligand surface density. The use of rigid and short linkers may also impede the conformational mobility of biomolecules, which may diminish reciprocal interaction between the interacting molecules. By contrast, long, flexible and distensible linkers such as poly(ethylene glycol) (PEG) provide increased mobility and orientational freedom that may favour optimal molecular recognition (FIG. 2a). It has been shown that linkers with a chain length of around 6–10 nm, corresponding to ~18–27 ethylene glycol units, provide a good balance between flexibility and narrow lateral resolution of the target site[79,80]. Additionally, during tip retraction, the stretching behaviour of a PEG linker provides a molecular fingerprint that helps identify specific unbinding or unfolding events.

Grafting ligands onto the AFM tip in a controlled orientation is an important point to consider in many studies. Methods that form covalent linkages via randomly distributed amino acid residues result in random orientation of the molecules on the AFM tip[77]. For site-specific attachment of molecules with controlled orientation, an appealing strategy based on the affinity between tetravalent nickel and histidine has been exploited for the immobilization of His_6-tagged proteins as sensor molecules on AFM tips[81] (FIG. 2a).

Proteins with a free cysteine or thiol-modified oligonucleotides can be easily immobilized at low micromolar concentrations using thiol–maleimide chemistry (FIG. 2a). The occurrence of free cysteines is rare in proteins and they spontaneously react with maleimide and bare gold surfaces, so coupling is performed in the presence of tris(2-carboxyethyl)phosphine (TCEP) that reduces disulfides to reactive sulfhydryl groups. Additional strategies to anchor proteins include an enzyme-assisted method relying on the sortase A transpeptidase obtained from *Staphylococcus aureus* that recognizes the LPXTG motif at the carboxy terminus of the target protein and ligates it to a second protein containing an amino-terminal oligo G motif[82], and copper(I)-assisted azide–alkyne cycloaddition (CuAAC)[83]. Both strategies allow site-specific tethering of biomolecules with controlled geometric loading configuration (FIG. 2b, right, and 2c).

Lastly, AFM-FS with chemically modified tips can map and quantify chemical heterogeneities on the cell surface, for example, by revealing hydrophobic nanodomains on fungal spores and on mycobacteria[84–86]. Typically, gold tips are modified with self-assembled monolayers of alkanethiols terminated with functional groups of interest such as hydroxyl or methyl terminals[84–87] (FIG. 2b, left).

Single-cell force spectroscopy

Central to SCFS is the preparation of physiologically relevant cell probes. Attachment of animal cells to tipless cantilevers — rather than cantilevers with tips whose sharp apex could either disturb or harm the cell — is often straightforward, and involves functionalizing the cantilever with specific proteins such as the mannose-binding lectin concanavalin A or extracellular matrix (ECM) proteins such as collagen or fibronectin[24,88]. Cell-Tak, a polyphenolic protein, may also be used[68,89,90]. However, suspending animal cells from the adherent state can be delicate as the detachment procedure can affect their adhesive or biophysical properties for time periods up to 1 h (REF.[91]).

Microbial cells require different protocols for cantilever attachment using either electrostatic[92,93] or hydrophobic[94] interactions, glue[95] or chemical fixation[96]. However, these approaches have limitations: first, multiple microbial cells might attach simultaneously to the cantilever, making data analysis more complex; and second, the cell may detach from the cantilever or be surface-altered during the procedures, leading to protein denaturation or cell death. A non-destructive protocol for producing single bacterial probes is to attach a colloidal particle onto a tipless cantilever, coat it with a bio-inspired polydopamine wet adhesive and, then, pick up a single cell lying on a substrate under optical control[71,97]. This methodology provides excellent control of the cell positioning and of the cell–substrate contact area during interaction, therefore enabling reproducible quantitative single-cell force measurements. For yeasts, tipless cantilevers coated with polydopamine or lectins are directly used without the need for a colloidal particle.

Another elegant method is fluidic force microscopy, which enables reversible immobilization of single cells using suction applied through microchannelled cantilevers by a pressure controller[98]. Fluidic force microscopy-based SCFS has been used to measure the adhesion between bacteria, yeast or mammalian cells and abiotic surfaces[99,100]. The technology has also proved very useful to study molecular interactions engaged in cell–cell association, providing new insights into the role of amyloid bonds in *Candida albicans* aggregation[101] and into the importance of stress-induced forces during yeast sexual reproduction[102].

The cell probe is used to record force–distance curves to sense interaction forces with a sample of interest, such as abiotic surfaces, protein-coated surfaces, other cells or tissues. To record an approach force–distance curve, the cell is brought into contact with the sample until a predefined contact force is reached. After a given time, typically ranging from 50 ms to several minutes, the cell is retracted and the force required to separate the cell from the sample is recorded to provide a signature of the detachment of the cell from the sample. Varying the contact force and the interaction time measures how cells initiate and strengthen adhesion to a given sample. With very small contact times between the cell probe and the sample, it is possible to detect single-molecule interactions of cells[24,88] as an alternative to SMFS.

Multiparametric imaging

Force volume imaging has long been a valuable AFM-FS method to map biophysical properties and biological interactions on surfaces, including live cells. Spatially resolved force–distance curves are collected on different areas of the sample. Each area can be divided into a certain number of pixels inside each of which a force–distance curve is recorded. The lateral resolution depends on the scan size, the number of pixels and the sharpness of the AFM tip. The adhesion force or elasticity can be extracted from each collected curve and displayed as grey

or coloured pixels. The pixel brightness directly reflects the magnitude of the measured parameter to generate adhesion force or elasticity maps of living cells[18,103].

Recent quantitative multiparametric AFM-FS-based imaging techniques can now record correlative images detailing structural, mechanical and chemical surface properties of living cells at high resolution and in a much shorter time than force volume imaging (FIG. 3). In the most widely used approach of peak-force tapping (PFT), the tip is oscillated with an amplitude of 100–1,000 nm and at a frequency of 0.25, 0.5, 1.0 or 2.0 kHz (FIG. 3a). In PFT mode, the cantilever is oscillated vertically with a sinusoidal waveform as opposed to the triangular waveform in conventional force volume mode. In addition, a feedback loop finely controls applied forces (the 'peak' forces) to afford gentle probing and successful correlated structural, mechanical and chemical imaging of soft biological samples with a high resolution up to 2,048 × 2,048 pixels. Initially, PFT was used with unmodified tips to study biological samples such as whole living cells, membrane proteins and amyloid fibrils but was later applied successfully to the study of chemical or specific molecular interactions using functionalized tips[54]. Multiparametric AFM-FS can also be combined with confocal imaging to characterize living animal cells. This is illustrated in FIG. 3b–f where an AFM tip functionalized with θ-toxin, which specifically targets cholesterol, probes the organization and mechanical properties of breast cancer cells by comparing co-culture of healthy (MCF10A) and malignant (MCF10CA1) cells. Malignant cells can appear softer with increased cholesterol[104] (FIG. 3d–f).

Multiparametric imaging offers several advantages over other AFM modes routinely used to force probe (bio)chemical sites, including higher spatial resolutions than classical topographic imaging modes, higher data acquisition speeds and greater fidelity in the correlation between adhesion, elasticity and topographic maps that are, above all, acquired simultaneously. Consequently, this method brings new exciting avenues to study the biochemical properties of cell surfaces and biomolecular interactions in relation to cellular function and morphology.

Current solutions to multiparametric imaging from various suppliers include PFT and quantitative imaging[49]. Although we do not discuss them in detail here, several

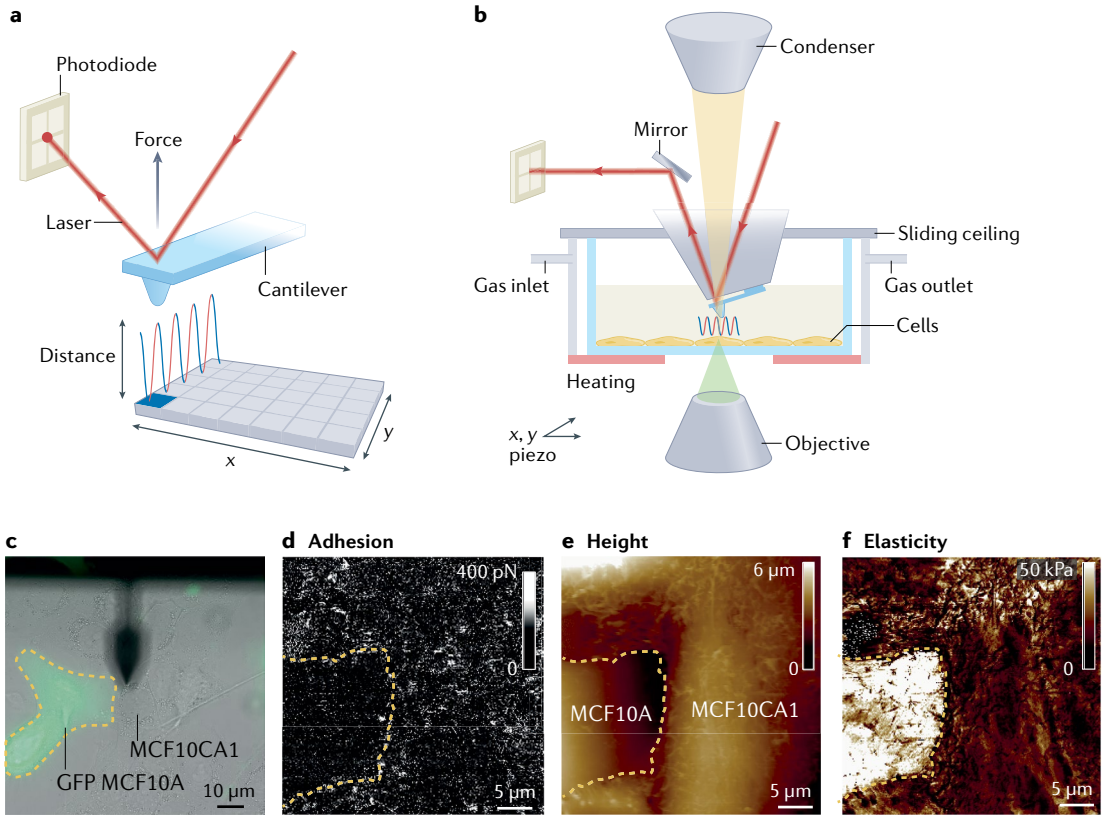

Fig. 3 | **Multiparametric AFM-FS and confocal imaging as a platform for probing the properties and interactions of living animal cells. a** | In peak-force tapping (PFT), the tip is oscillated in a sinusoidal manner while scanning the surface. On each pixel of the sample, a force curve is recorded, from which one can extract topography (height), elasticity and adhesion maps. **b** | Experimental set-up of a multiparametric atomic force microscopy (AFM)-based force spectroscopy (AFM-FS) and confocal imaging platform consisting of an AFM head placed on a confocal microscope. Cells are kept under incubator-like conditions (37 °C and with 5% CO_2) in a special cell-culture chamber, which prevents the culture-medium from evaporating. **c–f** | Fluorescence microscopy image of adjacent MCF10A (healthy) and MCF10CA1 (malignant) cells (part **c**) and correlated adhesion (part **d**), height (part **e**) and elasticity (part **f**) maps obtained by probing the cells using a θ-toxin functionalized AFM tip. GFP, green fluorescent protein. Parts **c–f** are reprinted from REF.[104], CC BY 4.0 (https://creativecommons.org/licenses/by/4.0/).

recent technological developments in the field of multiparametric imaging are worth mentioning. Ringing mode is a powerful new extension of PFT, where additional physical parameters such as adhesion height, pull-off neck height, detachment distance and energy loss can be measured with the regular sub-resonance tapping motion of the cantilever[105]. Ringing mode leverages the information stored in the resonance oscillations of the AFM cantilever after it detaches from the sample[106]. In comparison with conventional PFT mode, ringing mode uses the ringing at zero deflection and reduces interference artefacts that arise owing to interference of the laser.

Faster localization of binding sites can be achieved with topography and recognition imaging[107,108], in which tips functionalized with ligands are driven at resonance frequencies to simultaneously acquire topography and recognition images on cells[109]. Although this mode does not directly quantify interaction forces, it is equipped with the capability to conduct force spectroscopy experiments at binding sites localized in recognition images[110].

Also based on tapping mode, HarmoniX mode drives a special T-shaped cantilever with an offset tip at its resonance frequency to probe the tip–sample interaction and allows very high temporal resolution[111]. When the torsional harmonic cantilever is vibrated in tapping mode, a torque is created around it owing to the various interaction forces. The torsional vibrational signals are used to determine time-resolved tip–sample interaction forces, whereas the flexural vibrational signals are used for amplitude feedback to measure the topography akin to tapping mode AFM. As this technique leverages torsional vibrations that provide high sensitivity over a large range of frequencies, high-speed measurements can be performed with quantitative estimates of tip–surface rupture forces. The broad frequency range of torsional motion deciphers the higher overtones of the tip–sample interaction forces to reconstruct the tip–sample interaction wave shapes, from which a program constructs force–distance curves using the distance information in the vertical deflection signals. Finally, the mechanical response of the sample is obtained by fitting the force–distance curves to various physical models. Torsional harmonic AFM has been used to map the mechanical response of suspended silk fibres whose mesh-like architecture does not allow straightforward use of contact mechanics models[112]. Despite its ability to monitor the torsional movement of the AFM tip, the widespread applicability of torsional harmonic AFM is limited because of time-consuming fabrication and calibration of T-shaped cantilevers[113].

In photothermal off-resonance tapping mode, the cantilever is photothermally actuated by a laser beam. Therefore, the mass that needs to be excited includes only the cantilever and the tip, and not the *z*-piezo, which increases the measurement frequency by two orders of magnitude. This off-resonance technique has measured self-assembly driven by weak interactions in SAS6 protein rings that seed the centriole formation, using 50 pN force set point, 100 kHz frequency and 20 nm amplitude[114,115].

A recent modality, based on dynamic mechanical analysis, enables the study of viscoelastic properties of samples at the nanoscale (nanoDMA). Using subnanometre amplitudes when in contact, AFM nanoDMA works at small differential strain in the linear regime. This contrasts with traditional AFM approaches that rip the probe out of the surface on every cycle, a non-linear process that makes phase shift highly subject to variations in adhesion. It is a fast and sensitive technique allowing measurement of soft samples, in particular polymers, with high spatial (10–70 nm) and temporal (0.75 s per pixel) resolution. To circumvent problems such as creep, non-linear elastic responses, adhesion and long measurement times, nanoDMA can measure multiple frequencies simultaneously and decrease measurement time by avoiding a delay for creep relaxation[116]. Time-resolved forces can be acquired using multifrequency AFM, where additional information is contained in the deflection signal at frequencies other than at the excitation frequencies[117,118]. Multifrequency AFM provides high sensitivity and temporal resolution in the microsecond range by detecting high-frequency components of the cantilever and has helped measure protein flexibility and cell subsurface imaging with high spatial resolution[119–121].

Force-clamp spectroscopy

Force–distance curves, force volume imaging and multiparametric imaging rely on approach and retract cycles of the AFM tip. A different way to work is in force-clamp mode where, instead of the tip height, the force is ramped up to and kept at a constant level through continuous adaptation of the tip position by the piezoelectric scanner[122]. Force-clamp spectroscopy has mainly been used to study molecular responses, such as changes in protein conformation and unfolding of biomolecules under a constant applied force[123–125], but also to assess receptor–ligand bond lifetimes as a function of tensile loads[126,127]. Recently, force-clamp mode was implemented to study the mechanics of bacterial motorized nanomachines[128]. In the related height clamp mode, the tip is also subjected to a z-movement but, rather than the force, the height of the *z*-piezo is kept constant to monitor changes in force.

Cell elasticity measurements

To measure the mechanical properties of living cells, the cells are usually immobilized on a support and indented or compressed by the cantilever. Whereas the approach force–distance curve provides local insight into mechanical properties such as cell deformation or stiffness, the retraction force–distance curve provides local insight into the mechanical (de-)adhesion process of probe and sample. Recording arrays of force–distance curves makes it is possible to obtain spatially resolved maps of cell or tissue surface elasticity in relation to function[32]. This is particularly useful for mammalian cells whose stiffness can vary spatially owing to variations in height, cytoskeleton and dynamic remodelling[40,129–132]. Cellular stiffness varies by orders of magnitude depending on the cell type, from $E < 10$ kPa for soft mammalian cells to $E > 1$ MPa for rigid microbial cell walls[37–39].

Generally, the cantilever stiffness should match that of the cell because cantilevers that are too stiff may

Overtones
Waves of frequency that are a positive integer multiple of the frequency of the original wave.

Wave shapes
Oscillations of the cantilever.

Phase shift
A shift in the phase of an oscillation's sin wavefunction.

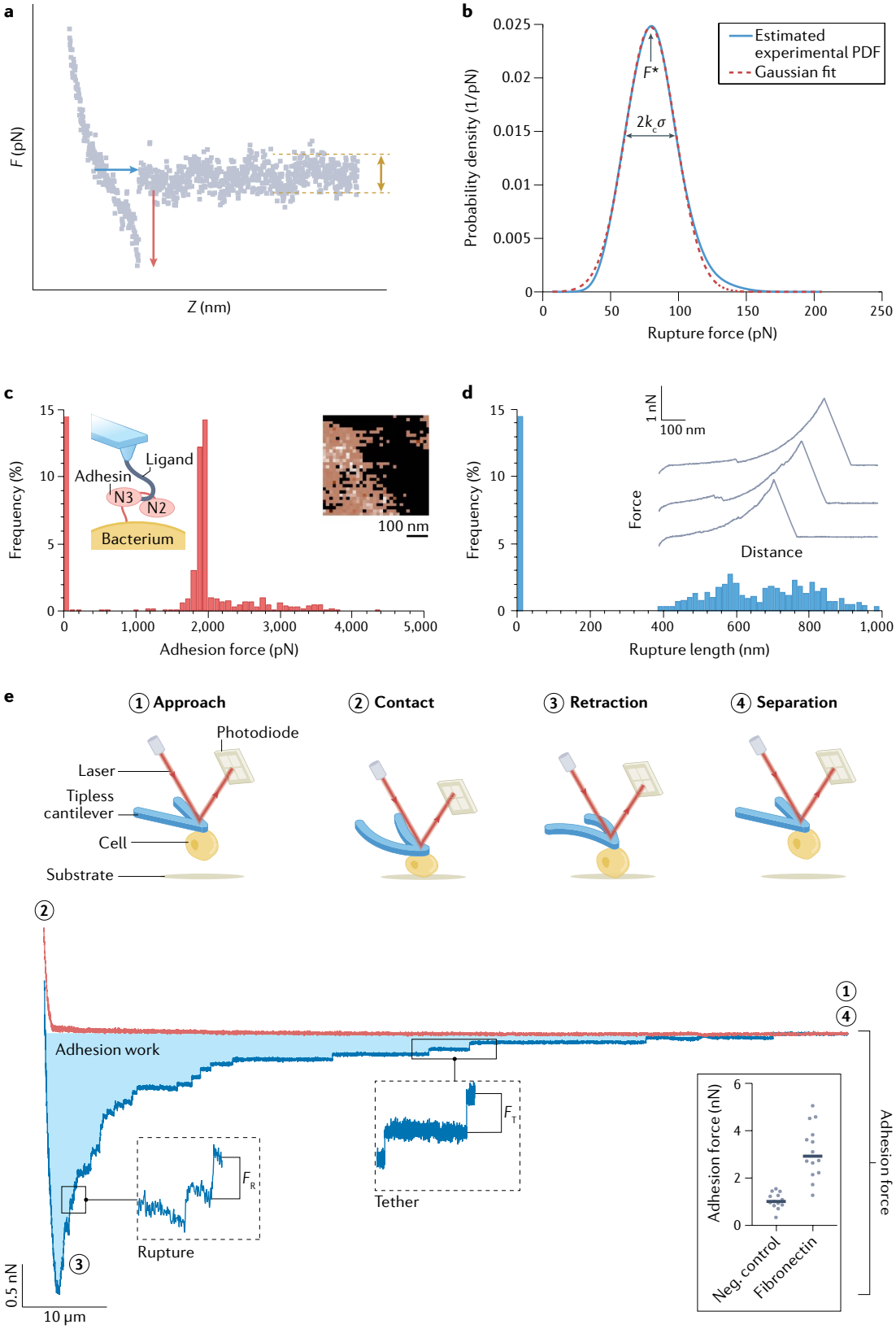

not detect the soft cell and cantilevers that are too soft and overbend cannot detect the cell stiffness properly. In addition, different probe geometries may be selected depending on the biological question to be answered. Commercially available pyramidal, conical or cylindrical tips can be used to indent cells locally, and thereby map mechanical heterogeneity over the cell surface. However, even small indentation forces often cause these sharp probes to penetrate deeply into the cell; coupled with the non-linear relationship between indentation depth and

◀ Fig. 4 | **Force–distance curve analysis. a** | Typical retract force–distance curve. The unbinding force is determined by the force difference between the rupture point and the baseline (red arrow), the unbinding length by the distance between the contact and the rupture points (blue arrow). From the thermal noise, the standard deviation of the unbinding force is calculated (yellow arrow). **b** | Experimental probability density function (PDF). A Gaussian fit (dashed line) determines the most probable unbinding force, in this case $F^* = 81$ pN (REF.[243]). Width σ of the unbinding force distribution reflects the stochastic nature of the unbinding process rather than the thermal noise. **c**,**d** | Analysis of single-molecule force spectroscopy (SMFS) data recorded on a living bacterium, i.e. of ClfA–fibrinogen (Fg) interactions on *Staphylococcus aureus*. Shown here is the adhesion force histogram plot (part **c**) with a force map (part **c**, inset; each coloured pixel signifies an adhesin–ligand binding event), and a rupture length histogram plot (part **d**) with representative adhesion force profiles (part **d**, inset) obtained by recording force–distance curves on a living cell with an atomic force microscopy (AFM) tip functionalized with Fg. **e** | Analysis of single-cell force spectroscopy (SCFS) data recorded for a living mammalian cell. (1) A single cell is immobilized on a tipless cantilever that has been functionalized with a cell adhesive, such as concanavalin A or a specific extracellular matrix (ECM) protein. (2) The cantilever-immobilized cell is then approached to a substrate of interest. Upon reaching a preset contact force, cantilever height is maintained for a defined contact time. (3,4) Subsequently, the cantilever is retracted vertically to separate cell and substrate. Force–distance curves show different features: from the approach force–distance curve (red) the apparent cell contact stiffness can be extracted; the retraction force–distance curve (blue) records the force with which the cantilever-immobilized cell (de-)adheres to the substrate, representing the maximum downward deflection of the cantilever. During detachment of the cell from the substrate, single receptor unbinding events are observed (ruptures). Ruptures are recorded when bonds formed between cytoskeleton-linked integrins and the substrate fail and allow quantification of the force a single adhesion receptor can withstand (F_R) at a particular loading rate. Tethers are recorded when a membrane tether extrudes from the cell body with a single integrin or multiple integrins at the tip of the tether and occur when the integrin linkage to the actomyosin cytoskeleton is either too weak to resist the mechanical load applied or non-existent. Adhesion forces of mammalian cells are commonly displayed in scattered dot plots, for example, as shown in the inset (solid lines indicate medians). F_T, the rupture force of the bond between a single tether-linked integrin and the substrate; k_c, effective spring constant of the whole system. Part **b** reprinted with permission from REF.[243], IOP. Parts **c** and **d** reprinted with permission from REF.[188], PNAS.

force, it makes it difficult to apply appropriate contact models to extract correct mechanical information from force–distance curves[116,133,134]. On the other hand, if the indentation is on the same length scale as the probe's roughness, it becomes difficult to estimate sample deformation. Further, as cells are often very flat, the surface effects of the underlying support need to be taken into consideration. Gluing micrometre-sized spherical probes to tipless cantilevers provides an alternative to sharp tips as the contact model of a sphere and a relatively smooth cell surface can be approximated more accurately using existing contact models. However, the restrictions of existing contact models such as small indentation, homogeneous materials, surface roughness and so on must be carefully studied and the AFM experiment designed appropriately so that the boundaries of the models are taken into consideration. In some cases, it may be useful to replace the AFM tip with a wedge to mechanically confine a cell between two parallel plates[135–138]. The wedge set-up allows the measurement of the mechanical properties of the entire cell and the application of simple contact models for mechanical analysis. For extensive and comprehensive reviews on cell elasticity measurements, see REFS[31,139].

In addition to the above traditional approaches, novel multiparametric imaging modes such as PFT and quantitative imaging can quantitatively map cell surface elasticity and topography simultaneously[140,141], as stated earlier, enabling for instance the imaging of cell wall stiffness and tensile strength during bacterial division and growth[141].

Binding probability of the molecular interaction
The ratio between the number of force–distance curves displaying a specific rupture event (or events) and the total number of force–distance curves recorded.

Measurement frequency range
The range of resonance frequency operation.

Results

We now describe how to extract and present relevant parameters for various AFM-FS modalities and sample types, starting with some general considerations on force–distance curve analysis for receptor–ligand interactions. We explain how to analyse SMFS and SCFS data obtained on cellular systems, and discuss model fitting to obtain quantitative information on molecular and cellular elasticity.

Data analysis

General considerations on force–distance curve analysis. In a typical SMFS experiment, at least 1,000 force–distance curves are recorded for one pulling velocity, allowing a robust statistical evaluation of the acquired data. For the detection of rupture (or adhesion) events arising from dissociating single biomolecular interactions, force jumps are depicted and a mean value and an accuracy of the rupture forces are calculated[142] (FIG. 4a). Two important pieces of information are the experimentally derived binding probability of the molecular interaction and the adhesion or rupture force, F, extracted from the force difference between the minimum of the rupture curve and the baseline. The measurement error or standard deviation is given by the noise amplitude that mainly arises from the thermal fluctuations of the cantilever. TABLE 1 shows the parameters that can be obtained from the curves.

The force resolution is mainly determined by the thermal noise of the cantilever, which is given by its spring constant. In addition, the resonance frequency, the quality factor and the measurement frequency range can also substantially contribute to the force resolution. Best results are therefore obtained with cantilevers exhibiting small spring constants — in the range of 0.01–0.10 N m^{-1} — and short lengths because they exhibit low force noise. Rupture forces gained from force–distance curves recorded at one pulling rate are collected to compute the distribution of rupture forces in the form of a histogram or a probability density function (PDF) (FIG. 4b). The most probable unbinding force, F^*, for one pulling velocity can then be extracted from the histogram or the PDF. Although representing force distributions using a histogram is simple, the binning width is arbitrary and jump discontinuities at the boundaries of each bin are unavoidable, and constructing a PDF may sometimes be a better choice. To compute the probability density of rupture forces, $p(F)$, each rupture event is assigned to its measurement error. In this way, data points with lower standard deviation are better weighted and contribute more to the outcome. The $p(F)$ for a force distribution is then calculated as follows:

$$p(F) = \sum_i \frac{1}{N\sigma_i\sqrt{2\pi}} \exp\left(-\frac{(F-\mu_i)^2}{2\sigma_i^2}\right) \quad (1)$$

where $p(F)$ is the estimate for the probability density that the bond will break at force F, μ_i is the rupture force and

Table 1 | **Additional parameters obtained from force–distance curves**

Parameter	Parameter determination	Notes
Binding probability of the molecular interaction	Calculated from the ratio between the number of force–distance curves displaying a signature of rupture (or ruptures) and the total number of force–distance curves recorded	Reflects the kinetic on-rate of the molecular interaction
Adhesion or rupture force, F	Determined from the force difference between the minimum of the rupture curve and the baseline	Reflects the force required to break the molecular interaction bond
Effective spring constant of the whole system, k_{eff}	Calculated from the slope immediately before the rupture event in the force–distance curve	Includes the contribution of the cantilever plus linker plus biological complex formed
Force loading rate (force increase over time)	Calculated from k_{eff} multiplied by the pulling velocity or from the slope immediately before the rupture event in the F versus t curve	Most important parameter when considering interaction dynamics
Rupture length	Determined as the distance between the rupture point and the contact point	Reflects the extended lengths of the involved molecules at the moment of rupture.

σ_i is the standard deviation, with the sum running over all N rupture events. The most probable rupture force can be determined by fitting a Gaussian function to the estimated PDF.

As we established above, the collected rupture forces can be represented as histograms or a PDF for a given data set recorded at one pulling rate. However, as the effective spring constant may vary, in particular in surfaces with inhomogeneous material properties such as cells, the data points for one pulling rate will spread over a whole range of loading rates and make the distribution harder to interpret. Theoretical papers usually treat force distributions for different loading rates and not pulling speeds. Distributions over a spectrum of loading rate, an approach called dynamic force spectroscopy (DFS) (see below), may give valuable insight into the energy landscape underlying the interaction under investigation.

Analysis of SMFS data from cellular systems. Applying SMFS to living cells implies recording force–distance curves using AFM tips terminated with cognate ligands. For microorganisms, parameters that are typically extracted from retraction force–distance curves are the maximum adhesion force and the rupture length of the last adhesion peak, the values of which are expressed as frequency histograms (FIG. 4c,d). For statistics and reproducibility, one should collect hundreds of force–distance curves using several ($n > 10$) cells and representative examples of retraction profiles should be shown (FIG. 4d, inset). For microbial data representation, one can either present histograms for individual cell probes or merge data from multiple cells into the same histogram plot, depending on the variability of the results. For spatially resolved SMFS imaging such as 32×32 curves on a 500 nm × 500 nm area, one may display the distribution of adhesion force values in the form of a two-dimensional map where the grey (or colour) scale of each pixel represents the adhesion strength (FIG. 4c, inset). This provides a valuable means to assess the surface density of cell surface receptors and whether they are clustered or randomly distributed. As further detailed below, when pulling on mammalian cells, receptors can detach from the cytoskeleton resulting in the extraction of a tether from the cell membrane.

As the bond strength is directly dependent on the loading rate, a DFS experiment explores the dynamics of receptor–ligand interactions. Adhesion force data are generated while varying the loading rate over several orders of magnitude. Theory (see below) and experiments have shown that the unbinding force between receptors and ligands increases with the loading rate. In the Bell–Evans model[143], rupture force increases log linearly with loading rate. A more recent model posited by Friddle et al.[144] accounts for non-linear trends in the relationship between rupture forces and loading rate arising from single bonds re-forming at low loading rates or asynchronous fluctuations of multiple independent interactions. These models apply to most receptor–ligand interactions where an increase in rupture force with loading rate is continuous. However, biological complexes forming catch bonds[145,146] can behave very differently in that binding is weak at low loading rate, but is dramatically enhanced above a critical loading rate value.

SCFS data analysis of cellular systems. In SCFS, force–distance curves are collected while varying contact forces and adhesion times between the cell probe and the target sample to probe both the overall cell adhesion force and the contribution of single adhesion molecules. As in SMFS, one should collect hundreds of force–distance curves for a single cell using several independent ($n > 10$) cells to obtain an appropriate statistical measure. Additionally, one should record spatially resolved force–distance curves on multiple spots of the target sample to avoid mechanically perturbing the cells. When recording the SCFS data, cell morphology and viability should be carefully monitored. Only force–distance curves recorded from the same cell morphology/state should be compared because cell morphology and state are tightly linked to each other and, for example, receptor–ligand interactions can depend on the cell state. Finally, a properly set up experiment should include characterizing sets of independently prepared cells and target samples.

For mammalian cells, the number of force–distance curves collected per single cell is considerably lower

Dynamic force spectroscopy
(DFS). An experiment where arrays of force–distance curves are recorded at varying pulling speeds.

Catch bonds
Specific bonds that increase lifetime with increasing force stressing them.

than bacteria and yeasts. This is mainly because mammalian cells commonly change morphology on the cantilever within 30–60 min, which changes the contact area between cell and substrate, the adhesion receptor surface density and cell mechanics[147]. In addition, the fluctuation of adhesion forces is greater between different cells than a single cell[148,149]. Mammalian cells may also respond to repetitive stressing by changing their adhesive or mechanical response[150]. To avoid such factors influencing the characterization of mammalian cells, the number of independent cells characterized per experimental condition should be at least ten. Owing to the small number of experiments per cell, the adhesion forces are usually displayed in a scattered dot plot showing individual data points and their median (FIG. 4e, right inset). The apparent stiffness of rounded animal cells can be extracted from the cantilever deflection upon compressing the cell onto the substrate[90,151]. In addition, the viscoelastic response of the compressed cell can be monitored[152] if the cantilever is maintained at a constant height after reaching a given contact force once the cell has approached a substrate. During the cell detachment process, complex adhesion patterns are often observed, with multiple rupture events describing the detachment of single or multiple adhesion receptors from their ligand (FIG. 4e). If the receptor remains anchored to the cell cortex, the rupture force quantifies the force a single adhesion receptor can withstand at the particular loading rate (FIG. 4e, left inset). If during retraction of the cell from the sample a single or a group of adhesion receptors detach from the cell cortex, they separate from the cell surface at the tip of a membrane tether (FIG. 4e, middle inset). This causes a force plateau in the force–distance curve and the force step of the plateau characterizes membrane properties such as membrane tension or fluidity. Finally, the lifetime of the receptor–ligand bond can be estimated by knowing the pulling velocity and the length of the tether[153,154]. Usually, the force distribution of rupture or tether events is displayed in histograms. For exhaustive SCFS reviews on animal and microbial cells, see REFS[24,155].

Model fitting

Molecular elasticity. In SMFS, a non-linear elongation force often precedes the rupture or adhesion peak. Analysis of the shape of this elongation provides valuable information on molecular mechanics. The elasticity of flexible cell surface molecules is commonly quantitatively described using the freely jointed chain (FJC) or worm-like chain (WLC) polymer extension models[156]. The FJC model describes a polymer that behaves similar to an ideal chain consisting of discrete segments that are connected by flexible joints. The segment length (or Kuhn length, l_k) provides a measure of the chain's overall stiffness. Extension of the polymer is limited by the contour length, L_c, which is related to the Kuhn length by $L_c = nl_k$. The extension x of the polymer can be expressed as a function of the tensile force F:

$$x(F) = L_c[\coth(Fl_k/k_bT) - k_bT/Fl_k] \quad (2)$$

where k_B is Boltzmann's constant and T is the absolute temperature.

In the WLC model's description of a polymer, although the backbone chain is continuously flexible and irregularly curved, it is linear on the scale of its persistence length, l_p, which is a quantitative measure of the polymer's elasticity. Therefore, polymers with a small l_p value tend to fold as coils. In the FJC model, the extension of the polymer is limited by its L_c. Here, F is expressed as a function of x:

$$F(x) = k_BT/l_p[0.25(1 - x/L_c)^{-2} + x/L_c - 0.25] \quad (3)$$

Extensible versions of both the FJC and the WLC models have been developed, where the molecular backbone of the polymers described can also be stretched. In the case of extensible FJC (called FJC+), the polymer is made up of n elastic springs (as opposed to inextensible segments) in series whose elasticity is defined in the parameter k_s. The extension–force relationship is given by:

$$x(F) = L_c[\coth(Fl_k/k_BT) - k_bT/Fl_k][1 + nF/k_sL_c] \quad (4)$$

Similarly, an extensible version of the WLC model (called WLC+) contains the stretch modulus term K_0 describing enthalpic stretching in addition to the entropic stretching represented by l_p. For high force regimes where the polymer is stretched significantly, the following formula is valid[157]:

$$x(F) = L_c[1 - 0.5(k_BT/Fl_p)^{0.5} + F/K_0] \quad (5)$$

In the context of AFM-FS studies, polymers that are well described by the WLC or WLC+ models include DNA and relatively unstructured proteins[16,130], whereas the FJC and FJC+ models better describe polysaccharides[158,159]. Finally, some molecules or bacterial appendages such as pili sometimes behave like classical Hookean springs[81,160,161], exhibiting a linear extension that cannot be fitted with either the WLC or the FJC models.

DFS fitting and interpretation. A theory depicting the dependence between rupture force and loading rate was developed using existing theory for overdamped kinetics[162]. DFS exploits this dependence to obtain kinetic and structural insights into intermolecular interactions. Intermolecular bond rupture in the time regime of DFS is a stochastic process. The likelihood of bond survival can be approached by a time-dependent probability under constant loading rate, which results in a distribution of dissociation forces for each loading rate. The most probable force, F, for dissociation taken from the maximum of these distributions scales linearly with the logarithm of loading rate. This phenomenological approach is commonly referred to as the Bell–Evans model[143]:

$$\langle F \rangle = f_\beta \left[\ln\left(\frac{r}{f_\beta k_{off}} \right) \right] \quad (6)$$

with $f_\beta = \frac{k_BT}{x_\beta}$, x_β the distance to the transition state along the projection of the applied force, r the loading rate and k_{off} the kinetic dissociation rate at zero force. For a single

Contour length
(L_c). The length of the linearly extended molecule without stretching the polymer backbone.

Persistence length
(l_p). A quantitative measure of a polymer's elasticity.

energy barrier separating the bound and the free state, the Bell–Evans model gives rise to a simple, linear correlation between F and ln(loading rate). Depending on the experimental setting, this correlation will depend on the pulling geometry and might only average a mean path of a complex energy landscape[163]. When several barriers are traversed, the relation between F and ln(r) will follow sequential linear regimes associated with abrupt slope changes. The dependence of the dissociation force on the loading rate allows exploring the energy landscape of the force-driven dissociation path.

Newer models predicting non-linear force spectra and equilibrium thermodynamics values, which include additional fit parameters such as the height, ΔG_β, and position, x_β, of the free energy barrier. Hummer and Szabo modified the phenomenological description given by the Bell–Evans model and described the bond's free energy landscape as a harmonic potential including a cusp-like surface[164,165], whereas Dudko et al.[166] performed a similar analysis using a linear-cubic energy surface, leading to:

$$\langle F\rangle \cong \frac{\Delta G_\beta}{\mu x_\beta}\left\{1-\left[\frac{k_B T}{\Delta G_\beta}\ln\left(\frac{k_{off}k_B T}{x_\beta r}\exp\left(\frac{\Delta G_\beta}{k_B T}+\gamma\right)\right)\right]^{\mu}\right\} \quad (7)$$

Here, $\mu = 2/3$ gives the quadratic free energy surface (Hummer–Szabo model), $\mu = 1/2$ gives the linear-cubic free energy surface (Dudko model) and γ the Euler constant. The model developed by Friddle et al.[144] includes reversible rebinding at low loading rates for soft springs. Two distinct unbinding regimes characterized by their loading rate ranges were developed: an equilibrium regime at low loading rates where bonds can re-form directly after unbinding, and a kinetic regime at high loading rates where bond rupture is irreversible. Both regimes are covered by a single fitting function, and the model is only applicable if both regimes are present. The fitting function also introduces the equilibrium force, F_{eq}, as an additional fit parameter. F_{eq} is the force at which dissociation and association are balanced as well as the lowest force at which a bond breaks irreversibly, thereby representing the point at which the equilibrium regime transitions into the kinetic regime. The rupture force F is given by:

$$\langle F\rangle = F_{eq} + f_\beta \ln\left(1+\frac{r}{f_\beta k_{off}}\exp\left[-\gamma-\frac{F_{eq}}{f_\beta}+\frac{k}{2}\frac{k_B T}{f_\beta^2}\right]\right) \quad (8)$$

where the equilibrium force $F_{eq} = \sqrt{2k\Delta G}$, with ΔG being the bond's equilibrium free energy and k the cantilever spring constant.

The Bell, Hummer–Szabo, Dudko and Friddle models yield two highly useful parameters. k_{off} and x_β derived from DFS experiments provide information about the transition velocity and the position of the dominant dissociation energy barriers: k_{off} represents the kinetic off-rate of the bond at zero force (that is, the inverse of the bond lifetime) and x_β the width of the dissociation energy potential. A simple method for directly determining force-dependent lifetimes from dissociation force histograms collected at different loading rates has been validated by Dudko et al.[167].

Cell mechanics. To quantify local mechanical properties of cellular samples, force–distance curves collected during indentation experiments are converted into force–indentation curves. Commercial AFM software programs commonly use the Hertz model to fit the contact region of the approach force–indentation curve and extract the sample elasticity or effective Young's modulus, E_{eff}. However, the Hertz model has the following in-built assumptions: the probe is a perfect sphere, the indented sample has a non-corrugated and planar surface, the indentation is perpendicular, there is no adhesion or friction between probe and sample, and the strain or tension of the cell cortex or wall linearly depends on Young's modulus. In addition, to avoid the contribution of the underlying support, cells should not be indented more than ~10% of their overall thickness. For spherical probes indenting the sample, the Hertz model considers that:

$$F = E_{eff}\cdot\left[(a^2+R_p^2)\cdot\ln\left(\frac{R_p+a}{R_p-a}\right)-2aR_p\right] \quad (9)$$

where F is the indenting force, a the contact radius and R_p the radius of the indenting probe. The contact radius a can be estimated from the indentation depth:

$$\delta = \frac{a}{2}\ln\left(\frac{R_p+a}{R_p-a}\right) \quad (10)$$

If the probe geometry differs from a sphere in the case of conical, cylindrical, parabolic or blunted pyramidal probes, the Hertz model has to be adapted to the specific geometry. There are other theoretical models to obtain mechanical information that are based on the Hertz model, such as the Derjaguin–Müller–Toporov and Johnson–Kendall–Roberts models, which have their specific advantages and limitations. Whereas the Derjaguin–Müller–Toporov model can be used for stiff materials with high E value and low adhesion between the sample and the probe, the Johnson–Kendall–Roberts model can be used when the adhesion between sample and probe is high. For an extensive review on cell mechanics models, see REF.[31].

Applications

Having described the range of AFM-FS methods available for molecular and cellular biology, we now survey their groundbreaking potential to address a wealth of problems with a series of studies focusing on viruses, bacteria, yeasts, mammalian cells and tissues. For an overview and key references see TABLE 2.

Force and dynamics of single bonds

The affinity of a receptor for its ligand is most often assessed by means of bulk equilibrium assays. However, living systems are highly dynamic and function out of equilibrium[168]. Cellular bonds are no exception as they

Table 2 | **Overview of currently available AFM-FS modalities to study living cells down to the single-molecule level, the wealth of information that can be obtained and representative references**

AFM-FS modalities for living cells	Information	Refs
Single-molecule force spectroscopy	Single bond strength	13,18,79,80,142,170, 173,180,185,186,243
	Molecular elasticity	16,81,130,158–160
	Receptor mapping	103,105,106,175
Dynamic force spectroscopy	Kinetics and thermodynamics of bonds	13,19,143,144,154,164–167, 169,170,173,176,212,213
	Stress-induced interactions	187,188,190,191
Force-clamp force spectroscopy	Catch bonds	126,127,146
	Protein unfolding/refolding	123,124,128
Single-cell force spectroscopy	Cell surface/host adhesion	13,68,71,88,90,97,149,172, 196–198,211,213,216
	Single adhesion receptor strength	24,149,153,196
	Cell–cell adhesion	24,88,101,102,140,194,195
	Anti-adhesion	193,194
Force spectroscopy-based indentation	Cell wall, cell membrane and cytoskeleton nanomechanics	31–35,37–39,137,152
Multiparametric force spectroscopy imaging	Correlative fluorescence force spectroscopy imaging	56,228,230,237,240–242
	Correlated topography, adhesion and elasticity	49,51–54,69,107,141
	Receptor density and clustering	49,109,110,212–216
	Chemical imaging	72,84–86

AFM-FS, atomic force microscopy-based force spectroscopy.

are exposed to various environmental fluctuations, including mechanical stress. The study of molecular and cellular interactions under force, when out of equilibrium, is most appropriate and physiologically relevant when it comes to systems that are exposed to physical stress and has strongly benefited from AFM-FS.

Since the mid 1990s, there has been tremendous progress in improving AFM-based SMFS and SCFS methodologies to decipher the strength and dynamics of individual cell adhesion bonds. Numerous pioneering works (for an overview, see REF.[18]) focused on cell adhesion molecules, such as cell adhesion proteoglycans[169], P-selectin/ligand complexes[170], discrete glycoprotein interactions involved in aggregating cells of *Dictyostelium discoideum*[88], integrin–fibronectin[171], *Escherichia coli* curli–fibronectin[172] and mycobacterial adhesin–ligand systems[103]. The binding strengths of the vast majority of receptor–ligand interactions reported in these studies, and in more recent ones, is in the range of 20–200 pN, and DFS showed that the bond strength generally increases with the loading rate in agreement with the Bell–Evans theory[19,173]. In addition, some adhesion proteins have a modular multidomain structure that plays various functional roles. The force needed to sequentially unfold their individual repeats ranges from 50 to 250 pN (REFS[174,175]), although some repeated domains can be more stable and unfold at 500 pN (REF.[140]).

Recently, a medically relevant application of AFM-FS experiments shed new light on the mechanisms of Lyme disease spirochaete motility[176]. This infectious disease is triggered by the spirochaete *Borrelia burgdorferi*, which expresses several adhesins that attach to host matrix proteins. During its infectious cycle, the pathogen migrates through different shear stress environments. AFM was combined with conventional bio-assays to understand the influence of adhesins on spirochaetal motility in low shear stress niches. SMFS using borrelial surface protein conjugated tips revealed that binding strength of decorin-binding proteins (DbpA and DbpB) was in the 25–75 pN range and was stronger for decorin than for laminin. The rupture force increases linearly with the log of the loading rate, as expected from the Bell–Evans theory (FIG. 5). Analysing the DFS data with the Bell–Evans model yields the kinetic k_{off} extrapolated to zero force, from which average bond lifetimes, τ, can be calculated according to $\tau = k_{off}^{-1}$. Stronger interaction forces and longer lifetimes for DbpA/B showed significantly stronger interaction with decorin than with laminin (FIG. 5a,b). The authors also used a binding probability assay to estimate the kinetic on-rate (k_{on}) of DbpA/B with decorin and with laminin (FIG. 5c). To this end, they varied the dwell time of the AFM tip on the surface, which is equal to the interaction time of the molecules on the tip with the molecules on the surface, and is the duration during which Dbp/ECM bonds may form. For DbpB–laminin, the binding probability increased with the dwell time following a well-known behaviour from which k_{on} can be gained. The binding probability of DbpA–laminin, however, first increased to saturation before decreasing in a quasi-exponential fashion because of successive dissociation of DbpA in the tip from laminin on the surface. Fitting the data using a pseudo first-order kinetics approximation yielded the unforced dissociation constant or lifetime. If the lifetime retrieved from the binding probability assay is much shorter than that of the DFS experiments, it is a clear indication that the bond becomes stabilized under force load as is the case for DbpA–laminin. Such bond behaviour is tailored for withstanding shear stress and might facilitate the dissemination of spirochaetes within vascular endothelia in blood vessels.

Catch bonds in staphylococcal adhesion

The streptavidin–biotin interaction has commonly been considered the strongest biological bond, sustaining forces of 100–250 pN as measured by AFM-FS and other force measuring techniques[177]. Recently, AFM-FS has enabled the discovery of non-covalent bacterial systems exhibiting much stronger binding strengths[178–180], including the cohesin–dockerin complex of cellulolytic bacteria[181,182] and the staphylococcal adhesins SdrG, ClfA and ClfB that engage in dock, lock and latch interactions[183] (FIG. 6). *Staphylococcus epidermidis* and *S. aureus* are two nosocomial pathogens that are of great medical concern as some strains are resistant to most antibiotics[184]. These bacteria are equipped with a series of adhesins that bind to their host proteins (FIG. 6a). AFM-based SMFS and SCFS studies have demonstrated that these bonds are capable of resisting tensile forces that can exceed ~2 nN (REFS[185,186]) (FIG. 6b), which is an order of magnitude greater than the strength of the biotin–avidin

Adhesins
Adhesion proteins on bacterial cell surfaces.

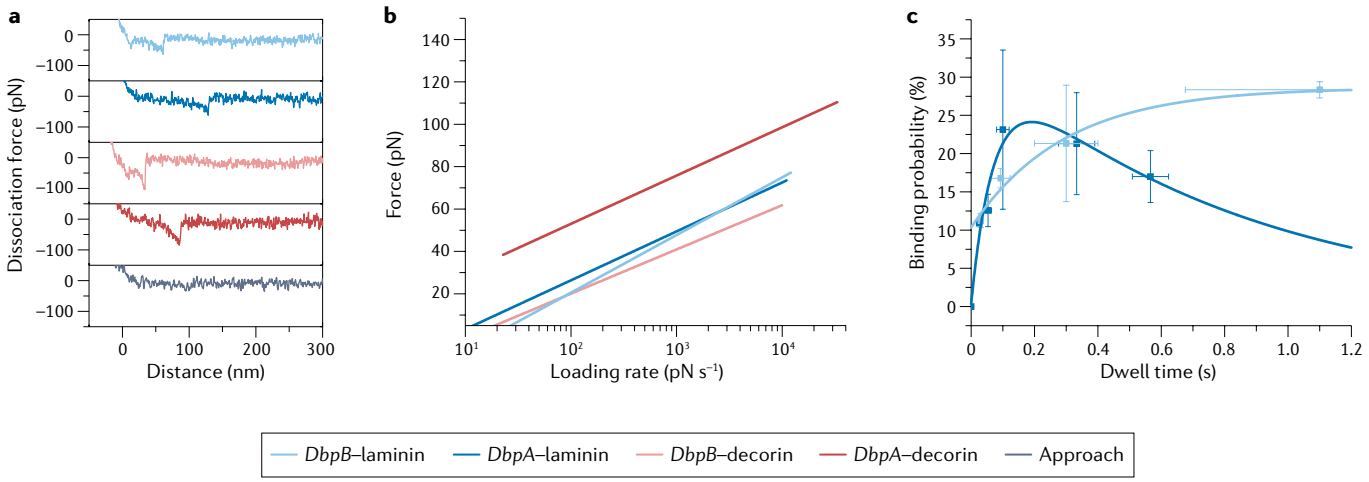

Fig. 5 | **Single-molecule Dbp–ECM bond analysis reveals force-tuned dissociation paths. a** | Force curves measured with dynamic force spectroscopy (DFS), yielding dissociation forces of individual decorin-binding protein (Dbp)–extracellular matrix (ECM) bonds. **b** | Maximum likelihood fits of individual dissociation force versus loading rate data (data points not shown) for single Dbp–ECM bonds. **c** | Binding probability assay. Binding probability for Dbp–ECM bond formation as a function dwell time. Reprinted from REF.[176], Springer Nature Limited.

interaction. This high strength is in contrast to the lower strength of the affinity of the complex measured at equilibrium and highlights the importance of probing bacterial bonds out of equilibrium.

A fascinating illustration of the influence of mechanics on cell behaviour[9] is the formation of catch bonds that, unlike classical slip bonds, reinforce under physical stress[146,187]. AFM-FS has shown that staphylococcal adhesins engage in catch-bond interactions with their ligands. In a first group of studies, DFS experiments revealed that ultra-strong binding by staphylococcal adhesins such as SdrG, ClfA and ClfB is further activated by tensile loading, leading to a force strengthening with increasing loads[188–190] (FIG. 6d). This finding strongly favours a catch-bond mechanism that enables staphylococci to firmly attach to their targets while resisting mechanical stresses associated with fluid flow or surface contacts.

The first direct proof of a staphylococcal catch bond came from AFM-based force-clamp experiments[127] (FIG. 6e,f). The bond lifetime between the staphylococcal surface protein SpsD and its ligand, fibrinogen (Fg), first grows with increasing tensile force before decreasing to behave as a slip bond beyond a critical force of ~1.1 nN, much stronger than other critical forces of purified bacterial complexes such as mannose–FimH complexes[191,192] and dockerin:cohesin complexes[182]. This biphasic transition is typical of catch-bond behaviour, which is consistent with the force-induced formation of long-lived hydrogen bonds between the ligand and the adhesin within the binding pocket. Stress-dependent catch bonds offer a means for pathogens to enhance their adhesion properties and, in turn, their ability to form biofilms under shear stress, for example, owing to flowing fluids (FIG. 6g). In summary, AFM-FS has contributed to showing that catch bonds might be more widespread among microorganisms than initially thought. Studying small compounds such as peptides and antibodies that are able to interfere with adhesion mechanisms may pave the way for the development of anti-adhesive therapies offering promising alternatives to conventional antibiotics that are becoming poorly efficient to fight multidrug-resistant pathogens[193]. For example, AFM identified a peptide derived from β-neurexin as a powerful inhibitor capable of efficiently blocking surface attachment, homophilic adhesion and biofilm accumulation mediated by the *S. aureus* SdrC adhesin. Molecular modelling suggested that this blocking activity originates from the binding of the peptide to a sequence of the adhesin involved in homophilic interactions[194].

Mammalian cell adhesion and mechanics

SCFS is widely applied to characterize how single mammalian cells initiate and strengthen adhesion to synthetic biomaterials such as hydrogels or protein fragments, natural biomaterials such as the ECM proteins fibronectin, collagens and laminin or other cells[195]. The adhesion initiation and strengthening processes of mammalian cells to ECM proteins, in particular, have been extensively studied by SCFS, such as fibronectin, which are driven by α/β heterodimeric integrins. By applying low contact forces and short contact times, SCFS reaches single-molecule sensitivity and quantifies binding rates of single adhesion integrins to their ligand. For example, it was recently shown that distinct fibronectin-binding α5β1 and αVβ3 integrins possess different ligand binding kinetics and thereby regulate adhesion initiation dynamics by competing for the same ligand[196,197]. By gradually increasing the contact time, and thereby increasing the time for the cell to interact with the substrate of interest, SCFS quantifies how single integrin receptors of the same type or different types synergize to strengthen cell adhesion over time as well as how intracellular adaptor and signalling proteins contribute to adhesion strengthening[149,197,198]. Molecular pathways regulating cell adhesion initiation and strengthening can be addressed by agonists of membrane proteins, inhibition of signalling

Slip bonds
Specific bonds that decrease lifetime with increasing force stressing them.

Integrins
A family of cell eukaryotic surface adhesion receptors that bind mainly to extracellular matrix (ECM) proteins.

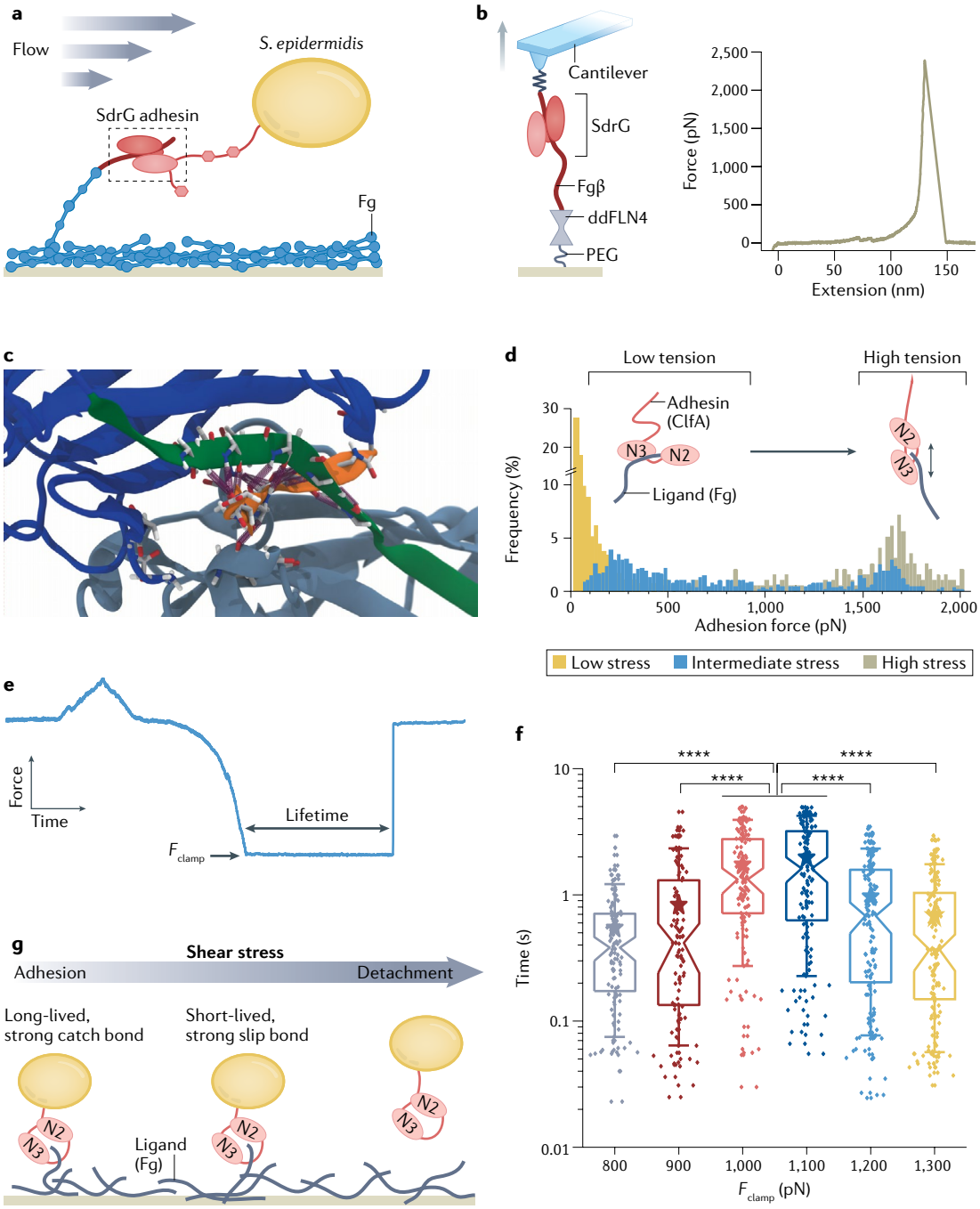

Fig. 6 | **Ultra-strong binding forces of staphylococcal adhesins. a** | Interaction between surface-exposed *Staphylococcus epidermidis* SdrG and the human blood circulatory protein fibrinogen (Fg). **b**,**c** | Atomic force microscopy (AFM) single-molecule force spectroscopy (SMFS) shows that the SdrG–Fg interaction ruptures at ~2 nN (part **b**) owing to an extensive hydrogen bond network that stabilizes the interaction between the SdrG binding site and the Fg β-chain amino-terminal peptide (part **c**). **d** | Mechanical activation of the strong interaction between *Staphylococcus aureus* ClfA (an orthologue of SdrG) and Fg. Increasing the loading rate promotes strengthening of the ClfA–Fg complex, with high rupture forces in the nN range, pointing to catch-bond behaviour. **e**–**g** | Unravelling catch-bond formation in a staphylococcal pathogen using AFM force-clamp experiments. Bond lifetime can be determined from the force–time curve via the persistence time before spontaneous unbinding of the complex directly under arbitrary clamp forces. **f** | Box plot showing biphasic behaviour of the lifetimes of interaction between the SpsD adhesin and Fg as a function of the clamping force. Catch-bond behaviour is observed where bond lifetime initially increases with force before a transition to slip-bond behaviour occurs. **g** | Bacterial binding to Fg under shear stress, relying on catch-bond behaviour exhibited by surface-exposed adhesins. ****, $P < 0.0001$; F_{clamp}, clamp force; PEG, poly(ethylene glycol). Panels **a**–**c** from REF.[186], Milles, L. F., Schulten, K., Gaub, H. E. & Bernardi, R. C. Molecular mechanism of extreme mechanostability in a pathogen adhesin. *Science* **359**, 1527–1533 (2018). Reprinted with permission from AAAS. Panel **d** reprinted with permission from REF.[188], PNAS. Panels **e** and **f** adapted from REF.[127], Springer Nature Limited.

molecules, engineered cell lines that express defined sets of adhesion receptors, substrates that are specific for distinct adhesion receptors and small molecules or antibodies blocking adhesion receptors.

A specific application of AFM-based SCFS is the study of adhesion receptor crosstalk[151,197] (FIG. 7). Single rounded cells are incubated on a cantilever functionalized with adhesion receptor-specific adhesives, such as ECM proteins, long enough for the adhesion receptors to initiate signalling. This allows quantification of the impact of the signalling initiated by cell adhesion to the cantilever on cell adhesion strengthening to the substrate. Using integrin-specific cantilever coatings has revealed that αV-class integrins induce signalling to promote ligand binding and clustering of a second class of fibronectin-binding integrins. In combination with total internal reflection microscopy, the adhesion receptor signalling-induced clustering has been optically resolved by monitoring the fluorescently labelled adhesion marker paxillin[197] (FIG. 7a). In addition, the high time and force resolution of SCFS has shown that distinct integrins respond to mechanical load by rapid signalling that induces the ligand binding of additional integrins in less than a second and has correlated the formation of α5β1 integrin–fibronectin catch bonds with changes in cellular signalling and a subsequent adhesion regulation[149]. However, if the mechanical load surpasses a threshold, the single integrin–fibronectin bond properties change to a slip bond and the load-dependent integrin activation fails.

AFM-FS is widely used to characterize the stiffness of single cells or tissues and has led to invaluable insights into how mechanical properties drive tissue development, regeneration and diseases. Spatially resolved time-lapse in vivo AFM-FS stiffness measurements combined with fluorescence microscopy in developing *Xenopus* have revealed rapid changes of mechanical properties in the developing brain (FIG. 7b) that drive the axonal growth and pathfinding in retinal ganglion cells to facilitate brain development[199,200]. In addition, scar

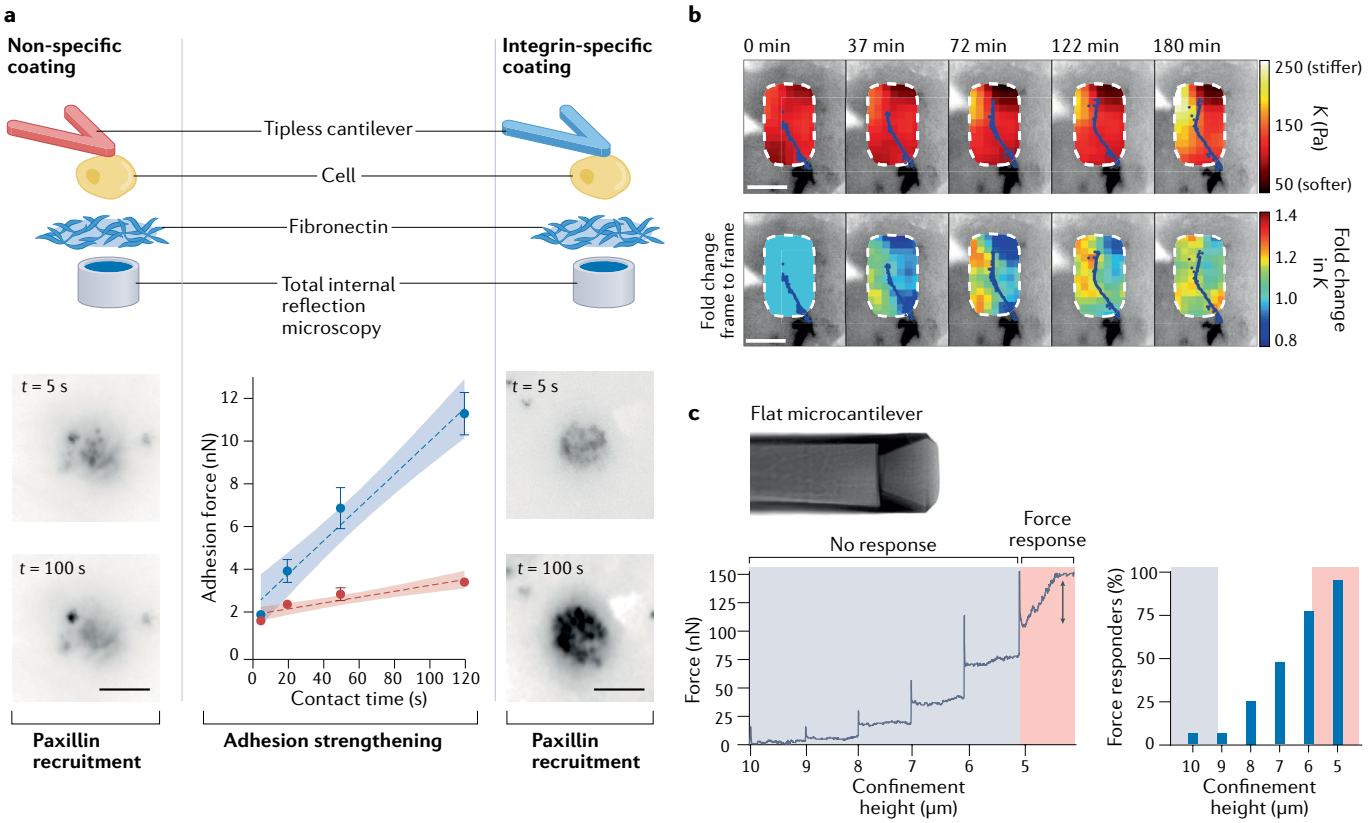

Fig. 7 | **Characterizing mammalian cell adhesion and mechanics using AFM-FS. a** | (Top) Set-up of a single-cell force spectroscopy (SCFS) integrin crosstalk experiment combined with total internal reflection microscopy. Atomic force microscopy (AFM) cantilevers are either coated with an unspecific adhesive, such as concanavalin A (orange), or an adhesion receptor-specific adhesive, such as the αV-class integrin-specific vitronectin (blue). Single fibroblasts, expressing paxillin–green fluorescent protein (GFP) as adhesion marker, are attached to the cantilever and allowed to adhere to a fibronectin-coated substrate for different contact times before quantifying their adhesion forces. (Bottom) During the contact time, the effect of αV-class integrin signalling on recruitment of paxillin–GFP can be observed (left and right panels) and correlated with adhesion strengthening (middle panel). Scale bars, 10 μm. **b** | (Top) Spatially resolved time-lapse stiffness measurements of *Xenopus* embryo brain overlaid with optical images of the brain. Outline of the fluorescently labelled optic tract neuron depicted in blue. Apparent elastic modulus, *K*, given in colour maps, and timestamp in minutes on each frame provides the elapsed time after the first image (bottom). Map of brain tissue stiffness changes over time in respect to previous time point. **c** | (Left) Representative response of a single rounded HeLa cell to stepwise compression (1-μm increment, 5-min interval) by the flat cantilever. (Right) Percentage of HeLa cells displaying a sustained force increase (>15 nN) as a function of height. AFM-FS, AFM-based force spectroscopy. Panel **a** reprinted from REF.[197], Springer Nature Limited. Panel **b** is adapted from REF.[199], CC BY 4.0 (https://creativecommons.org/licenses/by/4.0/). Panel **c** reprinted with permission from REF.[137], AAAS.

tissues in the neocortex and spinal cord are considerably softer than the surrounding tissue, which correlates with an enrichment of distinct ECM proteins and may provide a mechanical signal that limits neuronal growth[201].

Stiffness measurements of cancerous and healthy tissue reveal that tumour progression is related to an incremental stiffening of the tissue and that malignant breast cancer tissue shows a specific nanomechanical signature compared with healthy tissue[202–204]. Isolated cancer cells are typically softer than non-malignant cells[34,205] because they have defects in their ECM rigidity sensing[206]. The stiffness of the ECM in tumour stroma is about 10× higher than in healthy stroma[203] and is facilitated by the excessive deposition and cross-linking of ECM proteins, especially collagens[207]. Together with elegant cell biological experiments, AFM-FS has revealed that the increased stiffness of the ECM and the decreased stiffness of cancer cells correlates with the invasiveness and aggressiveness of the tumour[203,208].

Parallel plate assays were developed to study the mechanical properties of an entire cell and, hence, average over heterogeneous mechanical variabilities within the cell[209]. Parallel plate assays have shown that mitotic cells increase their osmotic pressure by recruiting myosin II to their cortical actin[135]. AFM-FS in combination with confocal microscopy has also revealed that the contractility of myosin is essential to resist against the deformation of the mitotic cells by the surrounding tissue, which itself has an impact on the duration of mitosis[136]. Recent AFM-FS experiments have revealed that non-mitotic cells also respond to the biophysical properties of their environment. It was shown that cells employ their nucleus as force ruler and, in case the nucleus is deformed, induce rapid signalling that increases cell contractility to withstand the externally applied forces[137] (FIG. 7c).

Virus–host cell interactions

Viral infection is initiated by the attachment of virus particles to the surface of their target host cells. Understanding these adhesive interactions is of great interest for the development of new antiviral therapeutics targeting viral surface proteins. AFM-FS with tips functionalized with individual virus particles, known as single-virus force spectroscopy, has enabled us to increase our understanding of virus interactions at the single-particle level. In an early work[210], the interactions between vesicular stomatitis virus and phosphatidylserine showed that virus attachment strength was dependent on the phospholipid composition of the probed membranes. In a study on the attachment of human rhinovirus particles to very low-density lipoprotein receptor (VLDLR), Rankl et al.[211] found that human rhinovirus virions formed multiple parallel interactions with VLDLRs grafted on an inert surface as well as on living cells. DFS analysis extracted the dissociation rate of single virus–receptor interactions. By varying the tip–sample contact time and monitoring the binding probability, the authors also extracted the kinetic association rate of the interactions. Reporting the ratio between the off-rate and on-rate yielded further insights into the overall affinity of the biomolecular partners in question.

Single-virus force spectroscopy-based multiparametric AFM imaging has recently provided a wealth of novel opportunities to study the molecular details of virus–host attachment. In a semantic study, Alsteens et al.[212] studied the kinetic and thermodynamic parameters of a complex virus–cell surface receptor complex using AFM-FS coupled to a confocal microscope. AFM tips functionalized with rabies virus were used to scan the surface of Madin–Darby canine kidney cells expressing fluorescently labelled avian tumour virus receptor A (TVA) to provide fundamental mechanistic insights into how viruses initiate infection in cells. The authors found that the binding probability of cells expressing TVA receptors was higher than wild-type cells and that the frequency of adhesion events was correlated to TVA receptor density[213]. Using single-virus force spectroscopy, Delguste et al.[214] demonstrated that the major envelope glycoprotein functions as a regulator of binding valency during both attachment and release steps and determines the binding, diffusion and release potential of virions at the cellular surface.

The molecular mechanism of interaction between reovirus T3SA$^+$ virions and α-sialic acid glycans immobilized on the surfaces of living cells was first unravelled using correlative AFM confocal microscopy (FIG. 8). More recently, the interaction between reovirus and β1 integrin was elucidated using similar approaches showing that the virus interacts specifically with the α2β1 integrin subunit with a high dependence on the presence of cations. As ligand affinity is guided by integrin conformation, which in turn depends on the presence of specific cations, it was demonstrated that the presence of Mn^{2+} triggers virions binding to integrins with a high affinity. As expected, nanoparticles functionalized with T3SA$^+$ infectious subvirion particles, which is likely mediated by the caveolin pathway, did not increase the blue fluorescence intensity of the blue fluorescent protein[215,216]. In summary, AFM-FS and confocal microscopy are a powerful platform to gain insight into virus–host interactions during the first stage of infection.

Reproducibility and data deposition

Here, we describe practices that are mandatory to generate reliable and robust force–distance data sets and analyses. Although standards for data deposition, data repositories and entry requirements have not been concretely established in the AFM force spectroscopy community, we strongly encourage minimal data sets to be made publicly available upon request, which should include the spring constant as well as the sensitivity and resonance frequency of the cantilevers used to produce the force–distance curves. Additional information may include raw rupture force, rupture length and loading rate data as well as information on the size of scanned areas and the numbers of pixels used. Preparation of such data is in a table format.

In a publication, it is essential to specify details about statistics and reproducibility. One should collect hundreds of force–distance curves using several ($n > 10$) cells and these numbers should be indicated in legends and/or text. For SMFS, force–distance curves should be recorded on different spots of the cell. To present the

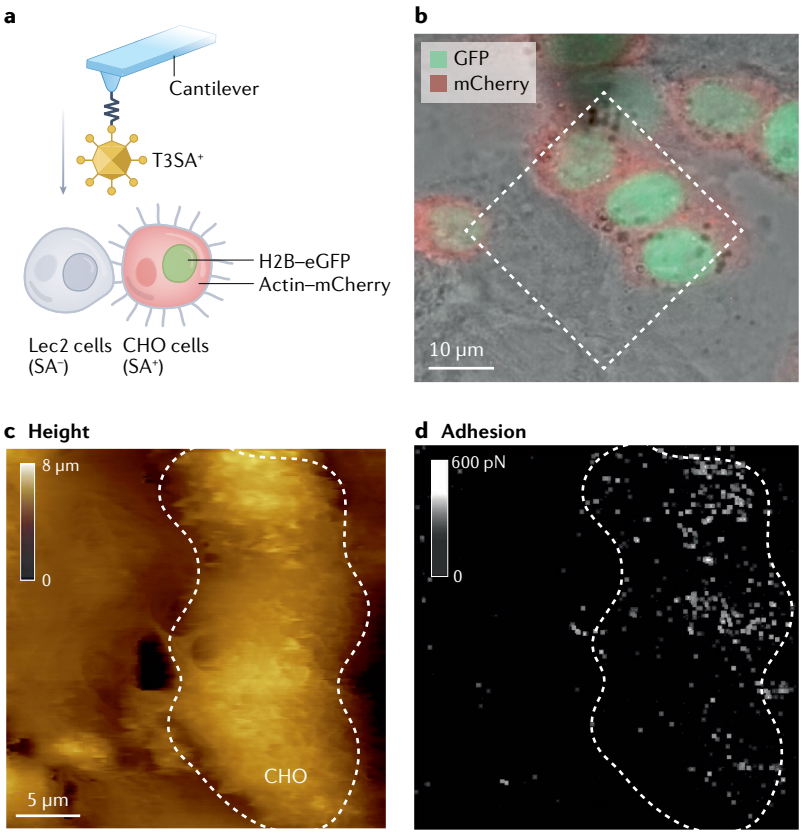

Fig. 8 | **Correlated AFM multiparametric and confocal imaging of single-virus binding interactions with living host cells. a** | Single virus-based multiparametric imaging and confocal microscopy reveal the distribution of binding events between the T3 reovirus immobilized on a tip and sialylated glycans on living cells. **b** | Overlay of transmitted light (non-fluorescent), green and red fluorescence images of a confluent layer of co-cultured Lec2 and fluorescent CHO cells. **c**,**d** | High-resolution correlative structural (part **c**) and adhesion (part **d**) images. Adhesion map shows interactions (bright white pixels) mainly on CHO cells (αSA-expressing cells), suggesting the establishment of specific of T3SA$^+$–αSA bonds on living cells. AFM, atomic force microscopy; eGFP, enhanced green fluorescent protein. Panels **a**–**d** reprinted from REF.[215], CC BY 4.0 (https://creativecommons.org/licenses/by/4.0/).

statistical ensemble of a measurement/condition, mean values and standard deviations or medians and 95% confidence intervals are typically provided together with the number of data points (n) and independent experiments considered. Representative examples of retraction profiles should be shown (FIG. 4d, inset).

To obtain an appropriate statistical measure in SCFS, one should collect hundreds of (for microbial cells) or up to 10 (for mammalian cells) force–distance curves for a single cell using several independent ($n > 10$) cells in a similar manner to SMFS. Additionally, one should record spatially resolved force–distance curves on multiple spots of the target sample to avoid mechanically perturbing the cells. When recording the SCFS data, one must carefully monitor the cell morphology and viability to later be able to compare only force–distance curves recorded from the same cell morphology/state. Experiments should also include characterizing sets of independently prepared cells and target samples. Finally, the approach speed, the contact time, the retraction speed and whether the cantilever's height or the applied force was maintained during the contact time strongly impact the recorded adhesion forces and must be reported[149,217].

Cell adhesion signatures can be difficult to interpret as multiple specific and non-specific forces can occur simultaneously. It is therefore essential to demonstrate the specificity of the targeted interaction. Control experiments showing such specificity should be performed, such as blocking cell surface receptors using target ligands that lack the binding site for adhesion receptors, antibodies, chemical compounds, free ligands or engineering cells in which the receptor under study is mutated or lacking[149,188,196–198].

In multiparametric imaging, the numbers of images collected and on how many independent cells should be stated, for example, in figure legends.

Finally, in the Methods section of a paper, it is critical to specify detailed protocols for sample and probe preparation so that the reader can judge the quality and biological relevance of the whole study.

Limitations and optimizations

Collecting reliable data by AFM-FS requires careful control of several parameters: the quality of sample and tip preparation procedures, the recording conditions, the accuracy of data collection and interpretation, and the cell type under study. Special care must be taken in analysing and interpreting force–distance curves.

Cantilever calibration

The correct calibration of the cantilever used is essential for all force spectroscopy applications. However, variabilities in instrumentation and experiments often lead to substantial deviations in spring constants of the same cantilever in different laboratories of up to 30%[218,219]. Hence, standard procedures and protocols for consistent cantilever calibrations should be established and indenting reference samples or deflecting cantilevers with well-defined mechanical properties can be used to check the calibration of the cantilever of interest[219,220].

Force–distance curve artefacts

Various artefacts in force–distance curves may appear and challenge subsequent analysis. These artefacts are usually easy to avoid using well-isolated systems and appropriate experimental set-ups. Below, we highlight a few common force–distance curve artefacts and how to mitigate or negate their appearance.

Baseline oscillations that interfere in photodiode readings sometimes arise owing to reflection of the laser from a highly reflective substrate such as gold. These oscillations may be mitigated by using a less reflective substrate or a more reflective cantilever, but usually do not pose a major problem to force–distance curve analyses provided that the oscillations are small. Another cause of baseline oscillations may be that the atomic force microscope is not adequately isolated from external vibrations, which would require the use of an anti-vibration platform and/or an acoustic hood for mitigation. Baseline tilt may occur owing to an off-centre photodiode. This is easily solved by re-aligning the photodiode and can be achieved using baseline tilt alignment

functions that are often available in commercial AFM data processing software.

Although thermal drift or hydrodynamic drag can skew the baseline and result in a gap between the approach and retraction force–distance curve, this does not typically pose major problems to force–distance curve analysis. To minimize baseline tilt, the system should be thermally equilibrated for typically ~15 min, but this can take longer depending on the temperature at which experiments are conducted.

An incomplete rupture during a force–distance curve retraction cycle may influence the approach cycle of the next force–distance curve, which can be solved by longer ramp length to allow complete separation between tip (and probe) and sample. Discontinuities in the contact portions of force–distance curves may arise when the tip punctures a sample or if the sample moves. This may be solved by decreasing the applied force or by improving the immobilization of the sample. A flat adhesion peak may arise from a strong adhesive interaction pulling the laser outside the photodiode range, which can be solved by aligning the laser such that a bigger deflection range can be recorded or by using a stiffer cantilever.

Other force–distance curve artefacts may also appear from the presence of impurities in the medium that interfere in the laser reflection or from tip movement that is too fast, often resulting in the production of uninterpretable curves.

Specific interactions

One of the difficulties in working with living cells as opposed to purified proteins is that various specific and non-specific interactions generally occur simultaneously at the cell surface. Because non-specific interactions usually act over short distances whereas biomolecules are usually stretched in specific interactions, the contours of the force–distance spectra produced by the two types of interactions are usually quite different, for example, biomolecules often show non-linear extension profiles and, depending on their sizes, biomolecular complexes would usually unbind over considerable distances. This means that during data analysis certain criteria may be used to discern specific from non-specific interactions, for example, by how well data can be fit by polymer extension models.

Although non-specific interactions can be filtered out during the data analysis step to some extent, they can largely be limited by taking appropriate measures during experimentation. An essential criterion is a clean substrate and sample preparation to expose non-specific interaction sites as little as possible. Note that adhesion forces measured for mammalian cells interacting with glass, mica or polydimethylsiloxane are often higher at contact times <60 s than when adhering to specific ECM proteins, which illustrates the necessity of completely covering the glass support with substrate for SCFS experiments[221]. Additionally, thorough control experiments are needed to decipher the contribution of specific and non-specific interactions to the measured forces, for example, using specific inhibitors. Today, advances in molecular biology and genetics also offer fast and elegant controls by genetically modifying cells, which carry mutated proteins of interest with either lacking or altered specific binding sites. Genetic modification can also be done with the target sample, for example, with mutated ligands, scrambled peptides or blocking proteins such as bovine serum albumin[188,197]. The genetic modification approach not only proves the specificity of the forces but enables the dissection of the molecular domains and binding sites at play to contribute to deciphering molecular mechanisms of adhesion[188].

Cell functionality

For any new cell type to be investigated by SMFS or SCFS, it is recommended to confirm that the immobilized cells on probes or substrates are alive and fully functional, ideally before and after a set of recordings. Viability can readily be assessed by fluorescent labelling to probe the membrane integrity or by incubation with propidium iodide or other commercially available live/dead cell staining kits. Functionality means that cells express properly the surface component of interest, for example, an integrin or an adhesin. Flow cytometry provides a fast tool to control cell surface expression of proteins, which should be regularly checked to ensure comparable SCFS results. It is crucial to evaluate whether modifications to genetically modified cells change the surface expression of the proteins of interest. If this is the case, fluorescence-activated cell sorting can be used to enrich the population of cells with physiological expression levels that are adequate for AFM-FS analysis.

During the course of an SCFS experiment, the immobilized cell might become poorly positioned, change its morphology or even detach from the probe. As SCFS is commonly coupled with optical microscopy, the position of the cell on the cantilever as well as state of the cell before, during and after an SCFS experiment can be monitored optically. In case undesired morphological changes are observed, the cell should be discarded. For microorganisms, well-defined adhesion events with extended ruptures are observed as a result of the stretching of cell surface macromolecules. If, during the analysis, the force–distance curve starts showing sharp adhesion peaks with very short ruptures, this could mean that the cell probe is damaged and one should restart the procedure with a fresh cell probe. For animal cells, one should compare specific and non-specific substrates to see whether they are different. If not, this could mean that the cell probe is altered and non-functional. Lastly, unlike in indentation experiments, it is recommended to limit the maximum contact force to 250 pN for microorganisms and 2,500 pN for animal cells to avoid cell surface damage.

Cell elasticity models

There are many potential sources of error that can limit the extent of validity and interpretation of existing models. Each theoretical model applied to fit the cell mechanics possesses advantages and limitations and specific assumptions that should be appropriately weighed to adequately choose the best model (see REF.[31]). For example, it has been shown that the shape of the AFM tip and indentation depth of the tip into the much softer cell must be carefully controlled, otherwise cell

elasticity measurements may be overestimated[31]. For stiffness measurements with sharp tips, the stiffness or modulus derived from localized indentation measurements will strongly depend on the exact area at which cell mechanical properties are measured, whereas using beads on the cantilever will average the mechanical properties over the contact area between the bead and the cell[40]. Additionally, substrate effects on elasticity measurements have to be considered for cells that are immobilized on either very soft or stiff substrates and may require the analytical model to be modified[222,223].

One can simultaneously use AFM and confocal microscopy to validate the most commonly employed forms of the Hertz model to extract elasticity from force–indentation curves on mammalian cells[224]. In the case of bacteria, the shape of the AFM tip as well as the indentation depth may not be as problematic during elasticity measurements. This is because bacteria possess relatively hard cell walls enabling them to resist deeper indentations of the AFM tip due to turgor pressure and cell wall mechanics. Nevertheless, although the absolute elasticity may become unreliable in certain experiments, relative changes in elasticity are typically more informative.

To address the uncertainties highlighted here, AFM is often combined with optical microscopy. Here, experiments that quantify mechanical properties of cells with fluorescently labelled structures of interest such as the cell membrane, nucleus or cytoskeletal filaments directly correlate the deformation of specific cellular architectures[225,226] with changes in apparent stiffness. Finally, note that the mechanical properties of cellular systems depend on the frequency at which they are probed and therefore should be characterized over a range of frequencies[227].

Statistical power

AFM-FS is inherently not a high-throughput single-cell analysis technique. Requirements such as the tip separation velocity being physiologically relevant (~1–10 μm s^{-1}), the tip separation distance being long enough to permit rupturing of all bonds between receptors on the tip and ligands on the sample surface, and that an array of force–distance curves must be collected over an adequately large cellular surface mean that collecting data for a single cell may take several minutes and up to half an hour. Therefore, the number of cells that can feasibly be analysed in a single experiment is generally small (approximately ten cells) in comparison with other single-cell techniques where data for hundreds or even thousands of cells are usually easily collected in a single experiment. When a large degree of phenotypic heterogeneity exists within a cell population, it may be an important consideration to use cell sorting techniques to enrich for target populations.

Outlook

The field of AFM-FS in the investigation of biomolecular and cellular interactions is young and the space for new discoveries remains immense. Many open scientific questions exist that could benefit from the methods reviewed in this Primer and we look forward to what the future holds. One pertinent question is how the sensing of mechanical stimuli occurs and how it is transduced into cellular responses ultimately playing a role in cell function (for recent reviews see REFS[6,7,9]). AFM-FS single-molecule and single-cell force probing methodologies are uniquely positioned to address this important issue in biology today. In particular, the increased availability of biocompatible AFM platforms that are coupled to epifluorescence, confocal or super-resolution optical microscopes will allow tracking intracellular events in response to force probing molecules on the cell surface.

AFM-FS and AFM topographic imaging are limited by their relatively low temporal resolution, and they only address the outer surface of cells. By contrast, super-resolution microscopy[228,229], also called optical nanoscopy, can probe the localization and motion of single molecules both outside and inside cells. Therefore, we expect that platforms combining AFM-FS with optical nanoscopy, some of which are currently commercially available, will address exciting new questions on the organization, dynamics and interactions of structures and machineries in single living cells (for a recent review see REF.[230]). Current optical nanoscopy modalities include stimulated emission depletion (STED) microscopy[231,232], PALM (photoactivated localization microscopy[233]), (d)STORM ((direct) stochastic optical reconstruction micropscopy[234]) and structured illumination microscopy[235]. They all aim at overcoming the diffraction limit of light, which imposes a finite magnification limit in conventional microscopy, by switching the fluorescence of a subpopulation of molecules on and off within a diffraction-limited area to enable molecules that are spatially indistinguishable from each other to be separated in time. In STED, the excitation beam is optically confined to a spot smaller than a diffraction-limited area, which is achieved by overlaying two beams: an excitation beam to induce fluorescence, and a doughnut-shaped STED beam for stimulated emission depletion and to inhibit fluorescence at the outer rim of the excitation beam. Only molecules at the centre of the excitation beam are allowed to fluoresce. The first STED microscope provided super-resolution images in three dimensions of living *E. coli* cells[236].

Correlative nanoscopy will hopefully allow the identification of specific cellular components while simultaneously probing their properties and interactions. For example, AFM was used to observe the structure of *E. coli* expressing a specific fusion protein whereas single-molecule localization PALM estimated the expression level and spatial distribution of the protein[237]. Another study combined STORM with SMFS AFM studies to study amino groups exposed on the cell membrane[238]. A proof-of-concept demonstration achieving simultaneous co-localized imaging of spatially correlated far-field super-resolution fluorescence microscopy and AFM was demonstrated with human bone osteosarcoma epithelial cells expressing plasma membrane transporter 1 (MCT1) tagged with an enhanced green fluorescent protein (EGFP) at the N terminus[239]. In 2012, a seminal study reported the combination of different AFM modes with STED, showing that STED and AFM can be used to produce high-resolution fluorescence imaging,

topographical imaging and nanomechanical imaging[240]. The choice of STED was motivated by the unique capabilities of the method, which include fast image acquisition. The same team demonstrated correlative STED AFM-based biomanipulation, showing the capability to monitor real-time responses of filament movements to mechanical force inside the cell and opening new perspectives for correlative AFM STED experiments[241]. Another study combined STED super-resolution imaging with AFM-FS to correlate nerve cell cytoskeletal structural organization with membrane physical properties, including the Young's modulus[242].

Although the future looks promising, several challenges still need to be overcome in the marriage of optical and force nanoscopy. First, the super-optical resolution is still accompanied by severe phototoxicity, which makes imaging of living cells highly challenging. Second, interference between the lasers employed by the two technologies complicates their simultaneous use. Third, limitations inherent to optical nanoscopy need to be overcome, such as the necessity to use compatible dyes and fluorophores. However, we are confident that, in the next years, combining AFM and optical nanoscopy will contribute to increasing our understanding of many cellular interactions and processes at single-molecular resolution.

Published online: 23 September 2021

1. Vogel, V. & Sheetz, M. Local force and geometry sensing regulate cell functions. *Nat. Rev. Mol. Cell Biol.* **7**, 265–275 (2006).
2. Schwartz, M. A. The force is with us. *Science* **323**, 588–589 (2009).
3. Roca-Cusachs, P., Conte, V. & Trepat, X. Quantifying forces in cell biology. *Nat. Cell Biol.* **19**, 742–751 (2017).
4. Petridou, N. I., Spiró, Z. & Heisenberg, C.-P. Multiscale force sensing in development. *Nat. Cell Biol.* **19**, 581–588 (2017).
5. Huse, M. Mechanical forces in the immune system. *Nat. Rev. Immunol.* **17**, 679–690 (2017).
6. Schwarz, U. S. Mechanobiology by the numbers: a close relationship between biology and physics. *Nat. Rev. Mol. Cell Biol.* **18**, 711–712 (2017).
7. Ladoux, B. & Mège, R.-M. Mechanobiology of collective cell behaviours. *Nat. Rev. Mol. Cell Biol.* **18**, 743–757 (2017).
8. Vining, K. H. & Mooney, D. J. Mechanical forces direct stem cell behaviour in development and regeneration. *Nat. Rev. Mol. Cell Biol.* **18**, 728–742 (2017).
9. Dufrêne, Y. F. & Persat, A. Mechanomicrobiology: how bacteria sense and respond to forces. *Nat. Rev. Microbiol.* **18**, 227–240 (2020).
10. Romani, P., Valcarcel-Jimenez, L., Frezza, C. & Dupont, S. Crosstalk between mechanotransduction and metabolism. *Nat. Rev. Mol. Cell Biol.* **22**, 22–38 (2021).
11. Kechagia, J. Z., Ivaska, J. & Roca-Cusachs, P. Integrins as biomechanical sensors of the microenvironment. *Nat. Rev. Mol. Cell Biol.* **20**, 457–473 (2019).
12. Uhler, C. & Shivashankar, G. V. Regulation of genome organization and gene expression by nuclear mechanotransduction. *Nat. Rev. Mol. Cell Biol.* **18**, 717–727 (2017).
13. Müller, D. J., Helenius, J., Alsteens, D. & Dufrêne, Y. F. Force probing surfaces of living cells to molecular resolution. *Nat. Chem. Biol.* **5**, 383–390 (2009).
14. Finer, J. T., Simmons, R. M. & Spudich, J. A. Single myosin molecule mechanics: piconewton forces and nanometre steps. *Nature* **368**, 113–119 (1994).
15. Schnitzer, M. J., Visscher, K. & Block, S. M. Force production by single kinesin motors. *Nat. Cell Biol.* **2**, 718–723 (2000).
16. Rief, M., Gautel, M., Oesterhelt, F., Fernandez, J. M. & Gaub, H. E. Reversible unfolding of individual titin immunoglobulin domains by AFM. *Science* **276**, 1109–1112 (1997).
17. Oesterhelt, F. et al. Unfolding pathways of individual bacteriorhodopsins. *Science* **288**, 143–146 (2000).
18. Hinterdorfer, P. & Dufrêne, Y. F. Detection and localization of single molecular recognition events using atomic force microscopy. *Nat. Methods* **3**, 347–355 (2006).
19. Evans, E. A. & Calderwood, D. A. Forces and bond dynamics in cell adhesion. *Science* **316**, 1148–1153 (2007).
20. Grandbois, M., Beyer, M., Rief, M., Clausen-Schaumann, H. & Gaub, H. E. How strong is a covalent bond? *Science* **283**, 1727–1730 (1999).
21. Ashkin, A., Dziedzic, J. M. & Yamane, T. Optical trapping and manipulation of single cells using infrared laser beams. *Nature* **330**, 769–771 (1987).
22. Neuman, K. C. & Nagy, A. Single-molecule force spectroscopy: optical tweezers, magnetic tweezers and atomic force microscopy. *Nat. Methods* **5**, 491–505 (2008).
23. Bian, K. et al. Scanning probe microscopy. *Nat. Rev. Methods Prim.* **1**, 1–29 (2021).
24. Helenius, J., Heisenberg, C.-P., Gaub, H. E. & Muller, D. J. Single-cell force spectroscopy. *J. Cell Sci.* **121**, 1785–1791 (2008).
25. Müller, D. J. & Dufrêne, Y. F. Atomic force microscopy as a multifunctional molecular toolbox in nanobiotechnology. *Nat. Nanotechnol.* **3**, 261–269 (2008).
26. Puchner, E. M. et al. Mechanoenzymatics of titin kinase. *Proc. Natl Acad. Sci. USA* **105**, 13385–13390 (2008).
27. del Rio, A. et al. Stretching single talin rod molecules activates vinculin binding. *Science* **323**, 638–641 (2009).
28. Ivanovska, I. L. et al. Bacteriophage capsids: tough nanoshells with complex elastic properties. *Proc. Natl Acad. Sci. USA* **101**, 7600–7605 (2004).
29. O'Callaghan, R., Job, K. M., Dull, R. O. & Hlady, V. Stiffness and heterogeneity of the pulmonary endothelial glycocalyx measured by atomic force microscopy. *Am. J. Physiol. Lung Cell Mol. Physiol.* **301**, L353–L360 (2011).
30. Howard, J., Grill, S. W. & Bois, J. S. Turing's next steps: the mechanochemical basis of morphogenesis. *Nat. Rev. Mol. Cell Biol.* **12**, 392–398 (2011).
31. Krieg, M. et al. Atomic force microscopy-based mechanobiology. *Nat. Rev. Phys.* **1**, 41 (2019).
32. Matzke, R., Jacobson, K. & Radmacher, M. Direct, high-resolution measurement of furrow stiffening during division of adherent cells. *Nat. Cell Biol.* **3**, 607–610 (2001).
33. Stewart, M. P. et al. Hydrostatic pressure and the actomyosin cortex drive mitotic cell rounding. *Nature* **469**, 226–230 (2011).
34. Cross, S. E., Jin, Y.-S., Rao, J. & Gimzewski, J. K. Nanomechanical analysis of cells from cancer patients. *Nat. Nanotechnol.* **2**, 780–783 (2007).
35. Iyer, S., Gaikwad, R. M., Subba-Rao, V., Woodworth, C. D. & Sokolov, I. Atomic force microscopy detects differences in the surface brush of normal and cancerous cells. *Nat. Nanotechnol.* **4**, 389–393 (2009).
36. Wirtz, D., Konstantopoulos, K. & Searson, P. C. The physics of cancer: the role of physical interactions and mechanical forces in metastasis. *Nat. Rev. Cancer* **11**, 512–522 (2011).
37. Gaboriaud, F., Bailet, S., Dague, E. & Jorand, F. Surface structure and nanomechanical properties of *Shewanella putrefaciens* bacteria at two pH values (4 and 10) determined by atomic force microscopy. *J. Bacteriol.* **187**, 3864–3868 (2005).
38. Touhami, A., Nysten, B. & Dufrêne, Y. F. Nanoscale mapping of the elasticity of microbial cells by atomic force microscopy. *Langmuir* **19**, 4539–4543 (2003).
39. Oh, Y. J. et al. Characterization of curli A production on living bacterial surfaces by scanning probe microscopy. *Biophys. J.* **103**, 1666–1671 (2012).
40. Mandriota, N. et al. Cellular nanoscale stiffness patterns governed by intracellular forces. *Nat. Mater.* **18**, 1071–1077 (2019).
41. Dufrêne, Y. F. et al. Imaging modes of atomic force microscopy for application in molecular and cell biology. *Nat. Nanotechnol.* **12**, 295–307 (2017).
42. Butt, H. J. et al. Imaging cells with the atomic force microscope. *J. Struct. Biol.* **105**, 54–61 (1990).
43. Hörber, J. K. et al. Investigation of living cells in the nanometer regime with the scanning force microscope. *Scanning Microsc.* **6**, 919–929 (1992); discussion 929–930.
44. Radmacher, M., Tillamnn, R. W., Fritz, M. & Gaub, H. E. From molecules to cells: imaging soft samples with the atomic force microscope. *Science* **257**, 1900–1905 (1992).
45. Butt, H.-J., Cappella, B. & Kappl, M. Force measurements with the atomic force microscope: technique, interpretation and applications. *Surf. Sci. Rep.* **59**, 1–152 (2005).
46. Cappella, B. & Dietler, G. Force–distance curves by atomic force microscopy. *Surf. Sci. Rep.* **34**, 1–104 (1999).
47. Radmacher, M., Cleveland, J. P., Fritz, M., Hansma, H. G. & Hansma, P. K. Mapping interaction forces with the atomic force microscope. *Biophys. J.* **66**, 2159–2165 (1994).
48. Heinz, W. F. & Hoh, J. H. Spatially resolved force spectroscopy of biological surfaces using the atomic force microscope. *Trends Biotechnol.* **17**, 143–150 (1999).
49. Dufrêne, Y. F., Martínez-Martín, D., Medalsy, I., Alsteens, D. & Müller, D. J. Multiparametric imaging of biological systems by force–distance curve-based AFM. *Nat. Methods* **10**, 847–854 (2013).
50. Adamcik, J., Berquand, A. & Mezzenga, R. Single-step direct measurement of amyloid fibrils stiffness by peak force quantitative nanomechanical atomic force microscopy. *Appl. Phys. Lett.* **98**, 193701 (2011).
51. Rico, F., Su, C. & Scheuring, S. Mechanical mapping of single membrane proteins at submolecular resolution. *Nano Lett.* **11**, 3983–3986 (2011).
52. Medalsy, I., Hensen, U. & Muller, D. J. Imaging and quantifying chemical and physical properties of native proteins at molecular resolution by force–volume AFM. *Angew. Chem. Int. Ed.* **50**, 12103–12108 (2011).
53. Heu, C., Berquand, A., Elie-Caille, C. & Nicod, L. Glyphosate-induced stiffening of HaCaT keratinocytes, a peak force tapping study on living cells. *J. Struct. Biol.* **178**, 1–7 (2012).
54. Alsteens, D. et al. High-resolution imaging of chemical and biological sites on living cells using peak force tapping atomic force microscopy. *Langmuir* **28**, 16738–16744 (2012).
55. Haupt, B. J., Pelling, A. E. & Horton, M. A. Integrated confocal and scanning probe microscopy for biomedical research. *ScientificWorldJournal* **6**, 1609–1618 (2006).
56. Newton, R. et al. Combining confocal and atomic force microscopy to quantify single-virus binding to mammalian cell surfaces. *Nat. Protoc.* **12**, 2275–2292 (2017).
57. Cumpson, P. J. & Hedley, J. Accurate analytical measurements in the atomic force microscope: a microfabricated spring constant standard potentially traceable to the SI. *Nanotechnology* **14**, 1279–1288 (2003).
58. Sader, J. E., Chon, J. W. M. & Mulvaney, P. Calibration of rectangular atomic force microscope cantilevers. *Rev. Sci. Instrum.* **70**, 3967–3969 (1999).
59. Hutter, J. L. & Bechhoefer, J. Calibration of atomic-force microscope tips. *Rev. Sci. Instrum.* **64**, 1868–1873 (1993).
60. Shoelson, B., Dimitriadis, E. K., Cai, H., Kachar, B. & Chadwick, R. S. Evidence and implications of inhomogeneity in tectorial membrane elasticity. *Biophys. J.* **87**, 2768–2777 (2004).

61. Lin, D. C., Dimitriadis, E. K. & Horkay, F. Robust strategies for automated AFM force curve analysis — I. Non-adhesive indentation of soft, inhomogeneous materials. *J. Biomech. Eng.* **129**, 430–440 (2006).
62. Lin, D. C., Dimitriadis, E. K. & Horkay, F. Robust strategies for automated AFM force curve analysis — II: adhesion-influenced indentation of soft, elastic materials. *J. Biomech. Eng.* **129**, 904–912 (2007).
63. Rudoy, D., Yuen, S. G., Howe, R. D. & Wolfe, P. J. Bayesian change-point analysis for atomic force microscopy and soft material indentation. *J. R. Stat. Society. C.* **59**, 573–593 (2010).
64. Benítez, R., Moreno-Flores, S., Bolós, V. J. & Toca-Herrera, J. L. A new automatic contact point detection algorithm for AFM force curves. *Microsc. Res. Tech.* **76**, 870–876 (2013).
65. Gavara, N. Combined strategies for optimal detection of the contact point in AFM force–indentation curves obtained on thin samples and adherent cells. *Sci. Rep.* **6**, 21267 (2016).
66. El Kirat, K., Burton, I., Dupres, V. & Dufrene, Y. F. Sample preparation procedures for biological atomic force microscopy. *J. Microsc.* **218**, 199–207 (2005).
67. Stewart, M. P., Toyoda, Y., Hyman, A. A. & Müller, D. J. Tracking mechanics and volume of globular cells with atomic force microscopy using a constant-height clamp. *Nat. Protoc.* **7**, 143–154 (2012).
68. Friedrichs, J., Helenius, J. & Muller, D. J. Quantifying cellular adhesion to extracellular matrix components by single-cell force spectroscopy. *Nat. Protoc.* **5**, 1353–1361 (2010).
69. Efremov, Y. M., Cartagena-Rivera, A. X., Athamneh, A. I. M., Suter, D. M. & Raman, A. Mapping heterogeneity of cellular mechanics by multi-harmonic atomic force microscopy. *Nat. Protoc.* **13**, 2200–2216 (2018).
70. Formosa, C. et al. Generation of living cell arrays for atomic force microscopy studies. *Nat. Protoc.* **10**, 199–204 (2015).
71. Beaussart, A. et al. Quantifying the forces guiding microbial cell adhesion using single-cell force spectroscopy. *Nat. Protoc.* **9**, 1049–1055 (2014).
72. Dufrêne, Y. F. Atomic force microscopy and chemical force microscopy of microbial cells. *Nat. Protoc.* **3**, 1132–1138 (2008).
73. Berquand, A. et al. Antigen binding forces of single antilysozyme Fv fragments explored by atomic force microscopy. *Langmuir* **21**, 5517–5523 (2005).
74. Kasas, S. & Ikai, A. A method for anchoring round shaped cells for atomic force microscope imaging. *Biophys. J.* **68**, 1678–1680 (1995).
75. Dufrêne, Y. F., Boonaert, C. J., Gerin, P. A., Asther, M. & Rouxhet, P. G. Direct probing of the surface ultrastructure and molecular interactions of dormant and germinating spores of *Phanerochaete chrysosporium*. *J. Bacteriol.* **181**, 5350–5354 (1999).
76. Bizzarri, A. R. & Cannistraro, S. The application of atomic force spectroscopy to the study of biological complexes undergoing a biorecognition process. *Chem. Soc. Rev.* **39**, 734–749 (2010).
77. Ott, W., Jobst, M. A., Schoeler, C., Gaub, H. E. & Nash, M. A. Single-molecule force spectroscopy on polyproteins and receptor–ligand complexes: the current toolbox. *J. Struct. Biol.* **197**, 3–12 (2017).
78. Müller, D. J. et al. Atomic force microscopy-based force spectroscopy and multiparametric imaging of biomolecular and cellular systems. *Chem. Rev.* https://doi.org/10.1021/acs.chemrev.0c00617 (2020).
79. Hinterdorfer, P., Baumgartner, W., Gruber, H. J., Schilcher, K. & Schindler, H. Detection and localization of individual antibody–antigen recognition events by atomic force microscopy. *Proc. Natl Acad. Sci. USA* **93**, 3477–3481 (1996).
80. Kienberger, F., Ebner, A., Gruber, H. J. & Hinterdorfer, P. Molecular recognition imaging and force spectroscopy of single biomolecules. *Acc. Chem. Res.* **39**, 29–36 (2006).
81. Dupres, V. et al. The yeast Wsc1 cell surface sensor behaves like a nanospring in vivo. *Nat. Chem. Biol.* **5**, 857–862 (2009).
82. Theile, C. S. et al. Site-specific N-terminal labeling of proteins using sortase-mediated reactions. *Nat. Protoc.* **8**, 1800–1807 (2013).
83. Chen, G., Ning, X., Park, B., Boons, G.-J. & Xu, B. Simple, clickable protocol for atomic force microscopy tip modification and its application for trace ricin detection by recognition imaging. *Langmuir* **25**, 2860–2864 (2009).
84. Alsteens, D., Dague, E., Rouxhet, P. G., Baulard, A. R. & Dufrêne, Y. F. Direct measurement of hydrophobic forces on cell surfaces using AFM. *Langmuir* **23**, 11977–11979 (2007).
85. Dague, E. et al. Chemical force microscopy of single live cells. *Nano Lett.* **7**, 3026–3030 (2007).
86. Viljoen, A., Viela, F., Kremer, L. & Dufrêne, Y. F. Fast chemical force microscopy demonstrates that glycopeptidolipids define nanodomains of varying hydrophobicity on mycobacteria. *Nanoscale Horiz.* **5**, 944–953 (2020).
87. Dorobantu, L. S., Bhattacharjee, S., Foght, J. M. & Gray, M. R. Atomic force microscopy measurement of heterogeneity in bacterial surface hydrophobicity. *Langmuir* **24**, 4944–4951 (2008).
88. Benoit, M., Gabriel, D., Gerisch, G. & Gaub, H. E. Discrete interactions in cell adhesion measured by single-molecule force spectroscopy. *Nat. Cell Biol.* **2**, 313–317 (2000).
89. Ng, G. et al. Receptor-independent, direct membrane binding leads to cell-surface lipid sorting and Syk kinase activation in dendritic cells. *Immunity* **29**, 807–818 (2008).
90. Taubenberger, A. V., Hutmacher, D. W. & Muller, D. J. Single-cell force spectroscopy, an emerging tool to quantify cell adhesion to biomaterials. *Tissue Eng. Part. B Rev.* **20**, 40–55 (2014).
91. Schubert, R. et al. Assay for characterizing the recovery of vertebrate cells for adhesion measurements by single-cell force spectroscopy. *FEBS Lett.* **588**, 3639–3648 (2014).
92. Le, D. T. L., Guérardel, Y., Loubière, P., Mercier-Bonin, M. & Dague, E. Measuring kinetic dissociation/association constants between *Lactococcus lactis* bacteria and mucins using living cell probes. *Biophys. J.* **101**, 2843–2853 (2011).
93. Ovchinnikova, E. S., Krom, B. P., van der Mei, H. C. & Busscher, H. J. Force microscopic and thermodynamic analysis of the adhesion between *Pseudomonas aeruginosa* and *Candida albicans*. *Soft Matter* **8**, 6454–6461 (2012).
94. Emerson, R. J. et al. Microscale correlation between surface chemistry, texture, and the adhesive strength of *Staphylococcus epidermidis*. *Langmuir* **22**, 11311–11321 (2006).
95. Bowen, W. R., Lovitt, R. W. & Wright, C. J. Atomic force microscopy study of the adhesion of *Saccharomyces cerevisiae*. *J. Colloid Interface Sci.* **237**, 54–61 (2001).
96. Razatos, A., Ong, Y. L., Sharma, M. M. & Georgiou, G. Molecular determinants of bacterial adhesion monitored by atomic force microscopy. *Proc. Natl Acad. Sci. USA* **95**, 11059–11064 (1998).
97. Beaussart, A. et al. Single-cell force spectroscopy of probiotic bacteria. *Biophys. J.* **104**, 1886–1892 (2013).
98. Guillaume-Gentil, O. et al. Force-controlled manipulation of single cells: from AFM to FluidFM. *Trends Biotechnol.* **32**, 381–388 (2014).
99. Potthoff, E. et al. Rapid and serial quantification of adhesion forces of yeast and mammalian cells. *PLoS ONE* **7**, e52712 (2012).
100. Potthoff, E., Ossola, D., Zambelli, T. & Vorholt, J. A. Bacterial adhesion force quantification by fluidic force microscopy. *Nanoscale* **7**, 4070–4079 (2015).
101. Dehullu, J. et al. Fluidic force microscopy demonstrates that homophilic adhesion by *Candida albicans* Als proteins is mediated by amyloid bonds between cells. *Nano Lett.* **19**, 3846–3853 (2019).
102. Mathelié-Guinlet, M. et al. Single-cell fluidic force microscopy reveals stress-dependent molecular interactions in yeast mating. *Commun. Biol.* **4**, 1–8 (2021).
103. Dupres, V. et al. Nanoscale mapping and functional analysis of individual adhesins on living bacteria. *Nat. Methods* **2**, 515–520 (2005).
104. Dumitru, A. C. et al. Label-free imaging of cholesterol assemblies reveals hidden nanomechanics of breast cancer cells. *Adv. Sci.* **7**, 2002643 (2020).
105. Sokolov, I. & Dokukin, M. E. Imaging of soft and biological samples using AFM ringing mode. *Methods Mol. Biol.* **1814**, 469–482 (2018).
106. Dokukin, M. E. & Sokolov, I. Nanoscale compositional mapping of cells, tissues, and polymers with ringing mode of atomic force microscopy. *Sci. Rep.* **7**, 11828 (2017).
107. Stroh, C. M. et al. Simultaneous topography and recognition imaging using force microscopy. *Biophys. J.* **87**, 1981–1990 (2004).
108. Stroh, C. et al. Single-molecule recognition imaging microscopy. *Proc. Natl Acad. Sci. USA* **101**, 12503–12507 (2004).
109. Chtcheglova, L. A., Waschke, J., Wildling, L., Drenckhahn, D. & Hinterdorfer, P. Nano-scale dynamic recognition imaging on vascular endothelial cells. *Biophys. J.* **93**, L11–L13 (2007).
110. Koehler, M. et al. Combined recognition imaging and force spectroscopy: a new mode for mapping and studying interaction sites at low lateral density. *Sci. Adv. Mater.* **9**, 128–134 (2017).
111. Sahin, O., Magonov, S., Su, C., Quate, C. F. & Solgaard, O. An atomic force microscope tip designed to measure time-varying nanomechanical forces. *Nat. Nanotechnol.* **2**, 507–514 (2007).
112. Cronin-Golomb, M. & Sahin, O. High-resolution nanomechanical analysis of suspended electrospun silk fibers with the torsional harmonic atomic force microscope. *Beilstein J. Nanotechnol.* **4**, 243–248 (2013).
113. Dong, M. & Sahin, O. A nanomechanical interface to rapid single-molecule interactions. *Nat. Commun.* **2**, 247 (2011).
114. Nievergelt, A. P., Banterle, N., Andany, S. H., Gönczy, P. & Fantner, G. E. High-speed photothermal off-resonance atomic force microscopy reveals assembly routes of centriolar scaffold protein SAS-6. *Nat. Nanotechnol.* **13**, 696–701 (2018).
115. Nievergelt, A. P., Brillard, C., Eskandarian, H. A., McKinney, J. D. & Fantner, G. E. Photothermal off-resonance tapping for rapid and gentle atomic force imaging of live cells. *Int. J. Mol. Sci.* **19**, E2984 (2018).
116. Dokukin, M. & Sokolov, I. High-resolution high-speed dynamic mechanical spectroscopy of cells and other soft materials with the help of atomic force microscopy. *Sci. Rep.* **5**, 12630 (2015).
117. Garcia, R. & Herruzo, E. T. The emergence of multifrequency force microscopy. *Nat. Nanotech* **7**, 217–226 (2012).
118. Lozano, J. R. & Garcia, R. Theory of multifrequency atomic force microscopy. *Phys. Rev. Lett.* **100**, 076102 (2008).
119. Dong, M., Husale, S. & Sahin, O. Determination of protein structural flexibility by microsecond force spectroscopy. *Nat. Nanotech* **4**, 514–517 (2009).
120. Shekhawat, G. S. & Dravid, V. P. Nanoscale imaging of buried structures via scanning near-field ultrasound holography. *Science* **310**, 89–92 (2005).
121. Tetard, L., Passian, A. & Thundat, T. New modes for subsurface atomic force microscopy through nanomechanical coupling. *Nat. Nanotech* **5**, 105–109 (2010).
122. Liu, B., Chen, W., Evavold, B. D. & Zhu, C. Accumulation of dynamic catch bonds between TCR and agonist peptide–MHC triggers T cell signaling. *Cell* **157**, 357–368 (2014).
123. Oberhauser, A. F., Hansma, P. K., Carrion-Vazquez, M. & Fernandez, J. M. Stepwise unfolding of titin under force-clamp atomic force microscopy. *Proc. Natl Acad. Sci. USA* **98**, 468–472 (2001).
124. Brujic, J., Hermans, R. I. Z., Garcia-Manyes, S., Walther, K. A. & Fernandez, J. M. Dwell-time distribution analysis of polyprotein unfolding using force-clamp spectroscopy. *Biophys. J.* **92**, 2896–2903 (2007).
125. Garcia-Manyes, S., Kuo, T.-L. & Fernández, J. M. Contrasting the individual reactive pathways in protein unfolding and disulfide bond reduction observed within a single protein. *J. Am. Chem. Soc.* **133**, 3104–3113 (2011).
126. Marshall, B. T. et al. Direct observation of catch bonds involving cell-adhesion molecules. *Nature* **423**, 190–193 (2003).
127. Mathelié-Guinlet, M. et al. Force-clamp spectroscopy identifies a catch bond mechanism in a Gram-positive pathogen. *Nat. Commun.* **11**, 5431 (2020).
128. Mignolet, J., Mathelié-Guinlet, M., Viljoen, A. & Dufrêne, Y. F. AFM force-clamp spectroscopy captures the nanomechanics of the Tad pilus retraction. *Nanoscale Horiz.* **6**, 489–496 (2021).
129. Lecuit, T. & Lenne, P.-F. Cell surface mechanics and the control of cell shape, tissue patterns and morphogenesis. *Nat. Rev. Mol. Cell Biol.* **8**, 633–644 (2007).
130. Oberhauser, A. F., Marszalek, P. E., Erickson, H. P. & Fernandez, J. M. The molecular elasticity of the extracellular matrix protein tenascin. *Nature* **393**, 181–185 (1998).
131. Fletcher, D. A. & Mullins, R. D. Cell mechanics and the cytoskeleton. *Nature* **463**, 485–492 (2010).
132. Chaudhuri, O., Parekh, S. H., Lam, W. A. & Fletcher, D. A. Combined atomic force microscopy and side-view optical imaging for mechanical studies of cells. *Nat. Methods* **6**, 383–387 (2009).
133. Kollmannsberger, P. & Fabry, B. Linear and nonlinear rheology of living cells. *Annu. Rev. Mater. Res.* **41**, 75–97 (2011).

134. Dimitriadis, E. K., Horkay, F., Maresca, J., Kachar, B. & Chadwick, R. S. Determination of elastic moduli of thin layers of soft material using the atomic force microscope. *Biophysical J.* **82**, 2798–2810 (2002).
135. Ramanathan, S. P. et al. Cdk1-dependent mitotic enrichment of cortical myosin II promotes cell rounding against confinement. *Nat. Cell Biol.* **17**, 148–159 (2015).
136. Cattin, C. J. et al. Mechanical control of mitotic progression in single animal cells. *Proc. Natl Acad. Sci. USA* **112**, 11258–11263 (2015).
137. Lomakin, A. J. et al. The nucleus acts as a ruler tailoring cell responses to spatial constraints. *Science* **370**, eaba2894 (2020).
138. Fläschner, G., Roman, C. I., Strohmeyer, N., Martinez-Martin, D. & Müller, D. J. Rheology of rounded mammalian cells over continuous high-frequencies. *Nat. Commun.* **12**, 2922 (2021).
139. Haase, K. & Pelling, A. E. Investigating cell mechanics with atomic force microscopy. *J. R. Soc. Interface* **12**, 20140970 (2015).
140. Formosa-Dague, C., Speziale, P., Foster, T. J., Geoghegan, J. A. & Dufrêne, Y. F. Zinc-dependent mechanical properties of *Staphylococcus aureus* biofilm-forming surface protein SasG. *Proc. Natl Acad. Sci. USA* **113**, 410–415 (2016).
141. Odermatt, P. D. et al. Overlapping and essential roles for molecular and mechanical mechanisms in mycobacterial cell division. *Nat. Phys.* **16**, 57–62 (2020).
142. Baumgartner, W., Hinterdorfer, P. & Schindler, H. Data analysis of interaction forces measured with the atomic force microscope. *Ultramicroscopy* **82**, 85–95 (2000).
143. Evans, E. & Ritchie, K. Dynamic strength of molecular adhesion bonds. *Biophys. J.* **72**, 1541–1555 (1997).
144. Friddle, R. W., Noy, A. & Yoreo, J. J. D. Interpreting the widespread nonlinear force spectra of intermolecular bonds. *Proc. Natl Acad. Sci. USA* **109**, 13573–13578 (2012).
145. Thomas, W. E., Vogel, V. & Sokurenko, E. Biophysics of catch bonds. *Annu. Rev. Biophys.* **37**, 399–416 (2008).
146. Sokurenko, E. V., Vogel, V. & Thomas, W. E. Catch-bond mechanism of force-enhanced adhesion: counterintuitive, elusive, but … widespread? *Cell Host Microbe* **4**, 314–323 (2008).
147. Pietuch, A. & Janshoff, A. Mechanics of spreading cells probed by atomic force microscopy. *Open. Biol.* **3**, 130084 (2013).
148. Dao, L., Gonnermann, C. & Franz, C. M. Investigating differential cell–matrix adhesion by directly comparative single-cell force spectroscopy. *J. Mol. Recognit.* **26**, 578–589 (2013).
149. Strohmeyer, N., Bharadwaj, M., Costell, M., Fässler, R. & Müller, D. J. Fibronectin-bound α5β1 integrins sense load and signal to reinforce adhesion in less than a second. *Nat. Mater.* **16**, 1262–1270 (2017).
150. Cui, Y. et al. Cyclic stretching of soft substrates induces spreading and growth. *Nat. Commun.* **6**, 6333 (2015).
151. Friedrichs, J., Helenius, J. & Müller, D. J. Stimulated single-cell force spectroscopy to quantify cell adhesion receptor crosstalk. *Proteomics* **10**, 1455–1462 (2010).
152. Radmacher, M. Measuring the elastic properties of living cells by the atomic force microscope. *Methods Cell Biol.* **68**, 67–90 (2002).
153. Krieg, M., Helenius, J., Heisenberg, C.-P. & Muller, D. J. A bond for a lifetime: employing membrane nanotubes from living cells to determine receptor–ligand kinetics. *Angew. Chem. Int. Ed.* **47**, 9775–9777 (2008).
154. Zhu, R. et al. Nanopharmacological force sensing to reveal allosteric coupling in transporter binding sites. *Angew. Chem. Int. Ed.* **55**, 1719–1722 (2016).
155. Dufrêne, Y. F. Sticky microbes: forces in microbial cell adhesion. *Trends Microbiol.* **23**, 376–382 (2015).
156. Janshoff, A., Neitzert, M., Oberdörfer, Y. & Fuchs, H. Force spectroscopy of molecular systems — single molecule spectroscopy of polymers and biomolecules. *Angew. Chem. Int. Ed.* **39**, 3212–3237 (2000).
157. Odijk, T. Stiff chains and filaments under tension. *Macromolecules* **28**, 7016–7018 (1995).
158. Rief, M., Oesterhelt, F., Heymann, B. & Gaub, H. E. Single molecule force spectroscopy on polysaccharides by atomic force microscopy. *Science* **275**, 1295–1297 (1997).
159. Marszalek, P. E., Oberhauser, A. F., Pang, Y. P. & Fernandez, J. M. Polysaccharide elasticity governed by chair–boat transitions of the glucopyranose ring. *Nature* **396**, 661–664 (1998).
160. Lee, G. et al. Nanospring behaviour of ankyrin repeats. *Nature* **440**, 246–249 (2006).
161. Beaussart, A. et al. Nanoscale adhesion forces of *Pseudomonas aeruginosa* type IV pili. *ACS Nano* **8**, 10723–10733 (2014).
162. Kramers, H. A. Brownian motion in a field of force and the diffusion model of chemical reactions. *Physica* **7**, 284–304 (1940).
163. Sedlak, S. M., Schendel, L. C., Gaub, H. E. & Bernardi, R. C. Streptavidin/biotin: tethering geometry defines unbinding mechanics. *Sci. Adv.* **6**, eaay5999 (2020).
164. Hummer, G. & Szabo, A. Free energy surfaces from single-molecule force spectroscopy. *Acc. Chem. Res.* **38**, 504–513 (2005).
165. Hummer, G. & Szabo, A. Kinetics from nonequilibrium single-molecule pulling experiments. *Biophys. J.* **85**, 5–15 (2003).
166. Dudko, O. K., Hummer, G. & Szabo, A. Intrinsic rates and activation free energies from single-molecule pulling experiments. *Phys. Rev. Lett.* **96**, 108101 (2006).
167. Dudko, O. K., Hummer, G. & Szabo, A. Theory, analysis, and interpretation of single-molecule force spectroscopy experiments. *Proc. Natl Acad. Sci. USA* **105**, 15755–15760 (2008).
168. Battle, C. et al. Broken detailed balance at mesoscopic scales in active biological systems. *Science* **352**, 604–607 (2016).
169. Dammer, U. et al. Binding strength between cell adhesion proteoglycans measured by atomic force microscopy. *Science* **267**, 1173–1175 (1995).
170. Fritz, J., Katopodis, A. G., Kolbinger, F. & Anselmetti, D. Force-mediated kinetics of single P-selectin/ligand complexes observed by atomic force microscopy. *Proc. Natl Acad. Sci. USA* **95**, 12283–12288 (1998).
171. Li, F., Redick, S. D., Erickson, H. P. & Moy, V. T. Force measurements of the α5β1 integrin–fibronectin interaction. *Biophys. J.* **84**, 1252–1262 (2003).
172. Oh, Y. J. et al. Curli mediate bacterial adhesion to fibronectin via tensile multiple bonds. *Sci. Rep.* **6**, 33909 (2016).
173. Merkel, R., Nassoy, P., Leung, A., Ritchie, K. & Evans, E. Energy landscapes of receptor–ligand bonds explored with dynamic force spectroscopy. *Nature* **397**, 50–53 (1999).
174. Alsteens, D. et al. Unfolding individual Als5p adhesion proteins on live cells. *ACS Nano* **3**, 1677–1682 (2009).
175. Alsteens, D., Garcia, M. C., Lipke, P. N. & Dufrêne, Y. F. Force-induced formation and propagation of adhesion nanodomains in living fungal cells. *Proc. Natl Acad. Sci. USA* **107**, 20744–20749 (2010).
176. Strnad, M. et al. Nanomechanical mechanisms of Lyme disease spirochete motility enhancement in extracellular matrix. *Commun. Biol.* **4**, 268 (2021).
177. Chilkoti, A., Boland, T., Ratner, B. D. & Stayton, P. S. The relationship between ligand-binding thermodynamics and protein–ligand interaction forces measured by atomic force microscopy. *Biophys. J.* **69**, 2125–2130 (1995).
178. Herman-Bausier, P. & Dufrêne, Y. F. Force matters in hospital-acquired infections. *Science* **359**, 1464–1465 (2018).
179. Viljoen, A., Mignolet, J., Viela, F., Mathelié-Guinlet, M. & Dufrêne, Y. F. How microbes use force to control adhesion. *J. Bacteriol.* **202**, e00125-20 (2020).
180. Milles, L. F. & Gaub, H. E. Extreme mechanical stability in protein complexes. *Curr. Opin. Struct. Biol.* **60**, 124–130 (2020).
181. Bernardi, R. C. et al. Mechanisms of nanonewton mechanostability in a protein complex revealed by molecular dynamics simulations and single-molecule force spectroscopy. *J. Am. Chem. Soc.* **141**, 14752–14763 (2019).
182. Liu, Z. et al. High force catch bond mechanism of bacterial adhesion in the human gut. *Nat. Commun.* **11**, 4321 (2020).
183. O'Connell, D. Dock, lock and latch. *Nat. Rev. Microbiol.* **1**, 171–171 (2003).
184. Foster, T. J. Immune evasion by staphylococci. *Nat. Rev. Microbiol.* **3**, 948–958 (2005).
185. Herman, P. et al. The binding force of the staphylococcal adhesin SdrG is remarkably strong. *Mol. Microbiol.* **93**, 356–368 (2014).
186. Milles, L. F., Schulten, K., Gaub, H. E. & Bernardi, R. C. Molecular mechanism of extreme mechanostability in a pathogen adhesin. *Science* **359**, 1527–1533 (2018).
187. Thomas, W. Catch bonds in adhesion. *Annu. Rev. Biomed. Eng.* **10**, 39–57 (2008).
188. Herman-Bausier, P. et al. *Staphylococcus aureus* clumping factor A is a force-sensitive molecular switch that activates bacterial adhesion. *Proc. Natl Acad. Sci. USA* **115**, 5564–5569 (2018).
189. Viela, F., Speziale, P., Pietrocola, G. & Dufrêne, Y. F. Mechanostability of the fibrinogen bridge between staphylococcal surface protein ClfA and endothelial cell integrin αVβ3. *Nano Lett.* **19**, 7400–7410 (2019).
190. Vitry, P. et al. Force-induced strengthening of the interaction between *Staphylococcus aureus* clumping factor B and Loricrin. *mBio* **8**, e01748-17 (2017).
191. Yakovenko, O. et al. FimH forms catch bonds that are enhanced by mechanical force due to allosteric regulation. *J. Biol. Chem.* **283**, 11596–11605 (2008).
192. Sauer, M. M. et al. Catch-bond mechanism of the bacterial adhesin FimH. *Nat. Commun.* **7**, 10738 (2016).
193. Geoghegan, J. A., Foster, T. J., Speziale, P. & Dufrêne, Y. F. Live-cell nanoscopy in antiadhesion therapy. *Trends Microbiol.* **25**, 512–514 (2017).
194. Feuillie, C. et al. Molecular interactions and inhibition of the staphylococcal biofilm-forming protein SdrC. *Proc. Natl Acad. Sci. USA* **114**, 3738–3743 (2017).
195. Krieg, M. et al. Tensile forces govern germ-layer organization in zebrafish. *Nat. Cell Biol.* **10**, 429–436 (2008).
196. Benito-Jardón, M. et al. αv-Class integrin binding to fibronectin is solely mediated by RGD and unaffected by an RGE mutation. *J. Cell Biol.* **219**, e202004198 (2020).
197. Bharadwaj, M. et al. αV-Class integrins exert dual roles on α5β1 integrins to strengthen adhesion to fibronectin. *Nat. Commun.* **8**, 14348 (2017).
198. Spoerri, P. M., Strohmeyer, N., Sun, Z., Fässler, R. & Müller, D. J. Protease-activated receptor signalling initiates α5β1-integrin-mediated adhesion in non-haematopoietic cells. *Nat. Mater.* **19**, 218–226 (2020).
199. Thompson, A. J. et al. Rapid changes in tissue mechanics regulate cell behaviour in the developing embryonic brain. *eLife* **8**, e39356 (2019).
200. Koser, D. E. et al. Mechanosensing is critical for axon growth in the developing brain. *Nat. Neurosci.* **19**, 1592–1598 (2016).
201. Moeendarbary, E. et al. The soft mechanical signature of glial scars in the central nervous system. *Nat. Commun.* **8**, 14787 (2017).
202. Lopez, J. I., Kang, I., You, W.-K., McDonald, D. M. & Weaver, V. M. In situ force mapping of mammary gland transformation. *Integr. Biol.* **3**, 910–921 (2011).
203. Acerbi, I. et al. Human breast cancer invasion and aggression correlates with ECM stiffening and immune cell infiltration. *Integr. Biol.* **7**, 1120–1134 (2015).
204. Plodinec, M. et al. The nanomechanical signature of breast cancer. *Nat. Nanotechnol.* **7**, 757–765 (2012).
205. Xu, W. et al. Cell stiffness is a biomarker of the metastatic potential of ovarian cancer cells. *PLoS ONE* **7**, e46609 (2012).
206. Yang, B. et al. Stopping transformed cancer cell growth by rigidity sensing. *Nat. Mater.* **19**, 239–250 (2020).
207. Maller, O. et al. Tumour-associated macrophages drive stromal cell-dependent collagen crosslinking and stiffening to promote breast cancer aggression. *Nat. Mater.* **20**, 548–559 (2021).
208. Mekhdjian, A. H. et al. Integrin-mediated traction force enhances paxillin molecular associations and adhesion dynamics that increase the invasiveness of tumor cells into a three-dimensional extracellular matrix. *Mol. Biol. Cell* **28**, 1467–1488 (2017).
209. Stewart, M. P. et al. Wedged AFM-cantilevers for parallel plate cell mechanics. *Methods* **60**, 186–194 (2013).
210. Carneiro, F. A. et al. Probing the interaction between vesicular stomatitis virus and phosphatidylserine. *Eur. Biophys. J.* **35**, 145–154 (2006).
211. Rankl, C. et al. Multiple receptors involved in human rhinovirus attachment to live cells. *Proc. Natl Acad. Sci. U S A* **105**, 17778–17783 (2008).
212. Alsteens, D. et al. Imaging G protein-coupled receptors while quantifying their ligand-binding free-energy landscape. *Nat. Methods* **12**, 845–851 (2015).
213. Alsteens, D. et al. Nanomechanical mapping of first binding steps of a virus to animal cells. *Nat. Nanotechnol.* **12**, 177–183 (2017).
214. Delguste, M. et al. Single-virus force spectroscopy discriminates the intrinsic role of two viral glycoproteins upon cell surface attachment. *Nano Lett.* **21**, 847–853 (2021).
215. Koehler, M. et al. Glycan-mediated enhancement of reovirus receptor binding. *Nat. Commun.* **10**, 4460 (2019).

216. Koehler, M. et al. Reovirus directly engages integrin to recruit clathrin for entry into host cells. *Nat. Commun.* **12**, 2149 (2021).
217. Oropesa-Nuñez, R., Mescola, A., Vassalli, M. & Canale, C. Impact of experimental parameters on cell–cell force spectroscopy signature. *Sensors* **21**, 1069 (2021).
218. te Riet, J. et al. Interlaboratory round robin on cantilever calibration for AFM force spectroscopy. *Ultramicroscopy* **111**, 1659–1669 (2011).
219. Schillers, H. et al. Standardized nanomechanical atomic force microscopy procedure (SNAP) for measuring soft and biological samples. *Sci. Rep.* **7**, 5117 (2017).
220. Sader, J. E. & White, L. Theoretical analysis of the static deflection of plates for atomic force microscope applications. *J. Appl. Phys.* **74**, 1–9 (1993).
221. Yu, M., Strohmeyer, N., Wang, J., Müller, D. J. & Helenius, J. Increasing throughput of AFM-based single cell adhesion measurements through multisubstrate surfaces. *Beilstein J. Nanotechnol.* **6**, 157–166 (2015).
222. Rheinlaender, J. et al. Cortical cell stiffness is independent of substrate mechanics. *Nat. Mater.* **19**, 1019–1025 (2020).
223. Gavara, N. & Chadwick, R. S. Determination of the elastic moduli of thin samples and adherent cells using conical atomic force microscope tips. *Nat. Nanotech* **7**, 733–736 (2012).
224. Harris, A. R. & Charras, G. T. Experimental validation of atomic force microscopy-based cell elasticity measurements. *Nanotechnology* **22**, 345102 (2011).
225. Staunton, J. R., Doss, B. L., Lindsay, S. & Ros, R. Correlating confocal microscopy and atomic force indentation reveals metastatic cancer cells stiffen during invasion into collagen I matrices. *Sci. Rep.* **6**, 19686 (2016).
226. Hobson, C. M. et al. Correlating nuclear morphology and external force with combined atomic force microscopy and light sheet imaging separates roles of chromatin and lamin A/C in nuclear mechanics. *Mol. Biol. Cell* **31**, 1788–1801 (2020).
227. Rico, F. et al. Probing mechanical properties of living cells by atomic force microscopy with blunted pyramidal cantilever tips. *Phys. Rev. E Stat. Nonlin Soft Matter Phys* **72**, 021914 (2005).
228. Xiao, J. & Dufrêne, Y. F. Optical and force nanoscopy in microbiology. *Nat. Microbiol.* **1**, 16186 (2016).
229. Schermelleh, L. et al. Super-resolution microscopy demystified. *Nat. Cell Biol.* **21**, 72–84 (2019).
230. Miranda, A. et al. How did correlative atomic force microscopy and super-resolution microscopy evolve in the quest for unravelling enigmas in biology? *Nanoscale* **13**, 2082–2099 (2021).
231. Hell, S. W. & Wichmann, J. Breaking the diffraction resolution limit by stimulated emission: stimulated-emission-depletion fluorescence microscopy. *Opt. Lett.* **19**, 780–782 (1994).
232. Hell, S. W. Microscopy and its focal switch. *Nat. Methods* **6**, 24–32 (2009).
233. Betzig, E. et al. Imaging intracellular fluorescent proteins at nanometer resolution. *Science* **313**, 1642–1645 (2006).
234. Rust, M. J., Bates, M. & Zhuang, X. Sub-diffraction-limit imaging by stochastic optical reconstruction microscopy (STORM). *Nat. Methods* **3**, 793–795 (2006).
235. Neil, M. A., Juskaitis, R. & Wilson, T. Method of obtaining optical sectioning by using structured light in a conventional microscope. *Opt. Lett.* **22**, 1905–1907 (1997).
236. Klar, T. A., Jakobs, S., Dyba, M., Egner, A. & Hell, S. W. Fluorescence microscopy with diffraction resolution barrier broken by stimulated emission. *Proc. Natl Acad. Sci. USA* **97**, 8206–8210 (2000).
237. Odermatt, P. D. et al. High-resolution correlative microscopy: bridging the gap between single molecule localization microscopy and atomic force microscopy. *Nano Lett.* **15**, 4896–4904 (2015).
238. Zhao, W. et al. Studying the nucleated mammalian cell membrane by single molecule approaches. *PLoS ONE* **9**, e91595 (2014).
239. Gómez-Varela, A. I. et al. Simultaneous co-localized super-resolution fluorescence microscopy and atomic force microscopy: combined SIM and AFM platform for the life sciences. *Sci. Rep.* **10**, 1122 (2020).
240. Harke, B., Chacko, J. V., Haschke, H., Canale, C. & Diaspro, A. A novel nanoscopic tool by combining AFM with STED microscopy. *Optical Nanoscopy* **1**, 3 (2012).
241. Chacko, J. V., Zanacchi, F. C. & Diaspro, A. Probing cytoskeletal structures by coupling optical superresolution and AFM techniques for a correlative approach. *Cytoskeleton* **70**, 729–740 (2013).
242. Curry, N., Ghézali, G., Kaminski Schierle, G. S., Rouach, N. & Kaminski, C. F. Correlative STED and atomic force microscopy on live astrocytes reveals plasticity of cytoskeletal structure and membrane physical properties during polarized migration. *Front. Cell Neurosci.* **11**, 104 (2017).
243. Rankl, C., Kienberger, F., Gruber, H., Blaas, D. & Hinterdorfer, P. Accuracy estimation in force spectroscopy experiments. *Jpn. J. Appl. Phys.* **46**, 5536–5539 (2007).

Acknowledgements
Work at the Université Catholique de Louvain was supported by the European Research Council (ERC) under the European Union's Horizon 2020 research and innovation programme (grant agreement no. 693630), the National Fund for Scientific Research (FNRS) and the Research Department of the Communauté française de Belgique (Concerted Research Action). Work at the Johannes Kepler University Linz was supported by the Austrian Science Fund (FWF) projects I 3173 (P.H. and Y.J.O.) and V584-BBL (Y.J.O.), and the Austrian National Foundation for Research, Technology, and Development and Research Department of the State of Upper Austria (Y.J.O.). D.A. and Y.F.D. are Research Associate and Research Director at the FNRS, respectively. The work at ETH Zurich was supported by the ETH Zurich (grant no. ETH-20 17-2), the Swiss National Science Foundation (grant no. 31003A_182587/1) and the NCCR Molecular Systems Engineering.

Author contributions
Introduction (A.V., M.M.-G., A.R., N.S., Y.J.O., P.H., D.J.M., D.A. and Y.F.D.); Experimentation (A.V., M.M.-G., A.R., N.S., Y.J.O., P.H., D.J.M., D.A. and Y.F.D.); Results (A.V., M.M.-G., A.R., N.S., Y.J.O., P.H., D.J.M., D.A. and Y.F.D.); Applications (A.V., M.M.-G., A.R., N.S., Y.J.O., P.H., D.J.M., D.A. and Y.F.D.); Reproducibility and data deposition (A.V., M.M.-G., A.R., N.S., Y.J.O., P.H., D.J.M., D.A. and Y.F.D.); Limitations and optimizations (A.V., M.M.-G., A.R., N.S., Y.J.O., P.H., D.J.M., D.A. and Y.F.D.); Outlook (A.V., M.M.-G., A.R., N.S., Y.J.O., P.H., D.J.M., D.A. and Y.F.D.); Overview of the Primer (Y.F.D.).

Competing interests
The authors declare no competing interests.

Peer review information
Nature Reviews Methods Primers thanks C. Heu, S. Kasas, O. Sahin and the other, anonymous, reviewer(s) for their contribution to the peer review of this work.

Publisher's note
Springer Nature remains neutral with regard to jurisdictional claims in published maps and institutional affiliations.

doi: 10.1038/s43586-021-00067-6; Article citation ID: 2021 1:64 For the Primer, visit doi: 10.1038/10.1038/s43586-021-00062-x

PrimeView

Force spectroscopy of single cells using atomic force microscopy

Among atomic force microscopy (AFM) techniques, AFM-based force spectroscopy (AFM-FS) investigates the strength and dynamics of cell adhesion, spatially maps surface receptors and quantifies how cells regulate their mechanical and adhesive properties to give us insight into how mechanical forces influence cellular processes.

Experimentation

An atomic force microscope consists of a sharp tip, typically ended in a nanometre-sized apex, attached to the free end of a soft cantilever. When the tip comes into contact with the sample surface, the tip–sample interactions cause the cantilever to deflect, which is recorded via a laser beam that is reflected onto a position-sensitive photodiode. The cantilever deflection is directly proportional to the force acting between the tip and the sample. AFM-FS acquires force–distance or force–time curves, in which the force applied or experienced by the AFM tip is monitored as a function of either the distance between the tip and the sample surface or time. As the tip approaches the sample, comes into contact with it, pushes on it and finally retracts, the sample's biophysical properties such as elasticity and adhesion can be obtained. Functionalizing the tip or the cantilever with cells, biomolecules or chemical groups enables measurement of specific biological and chemical interactions both at the single-cell and single-molecule levels. AFM-FS can measure forces ranging from a few piconewtons to several hundreds of nanonewtons and stiffnesses from about 100 to 10^9 pascals.

Results

When the tip makes contact with the surface and pushes on it, the sample elastic properties such as deformation, elasticity and stiffness can be derived from theoretical contact models. As the tip is moved upward, the cantilever relaxes and the adhesion force of the system can be determined. By functionalizing the AFM probe with biomolecules (ligands) in single-molecule FS or with cells (eukaryotic or prokaryotic) in single-cell FS, the strength of molecular and cellular interactions, respectively, can be measured. Two important parameters to determine are the experimentally derived binding probability of the molecular interaction and the adhesion force.

Applications

The many modalities of AFM-FS enable the gathering of a wealth of mechanical and adhesive information from living cells.

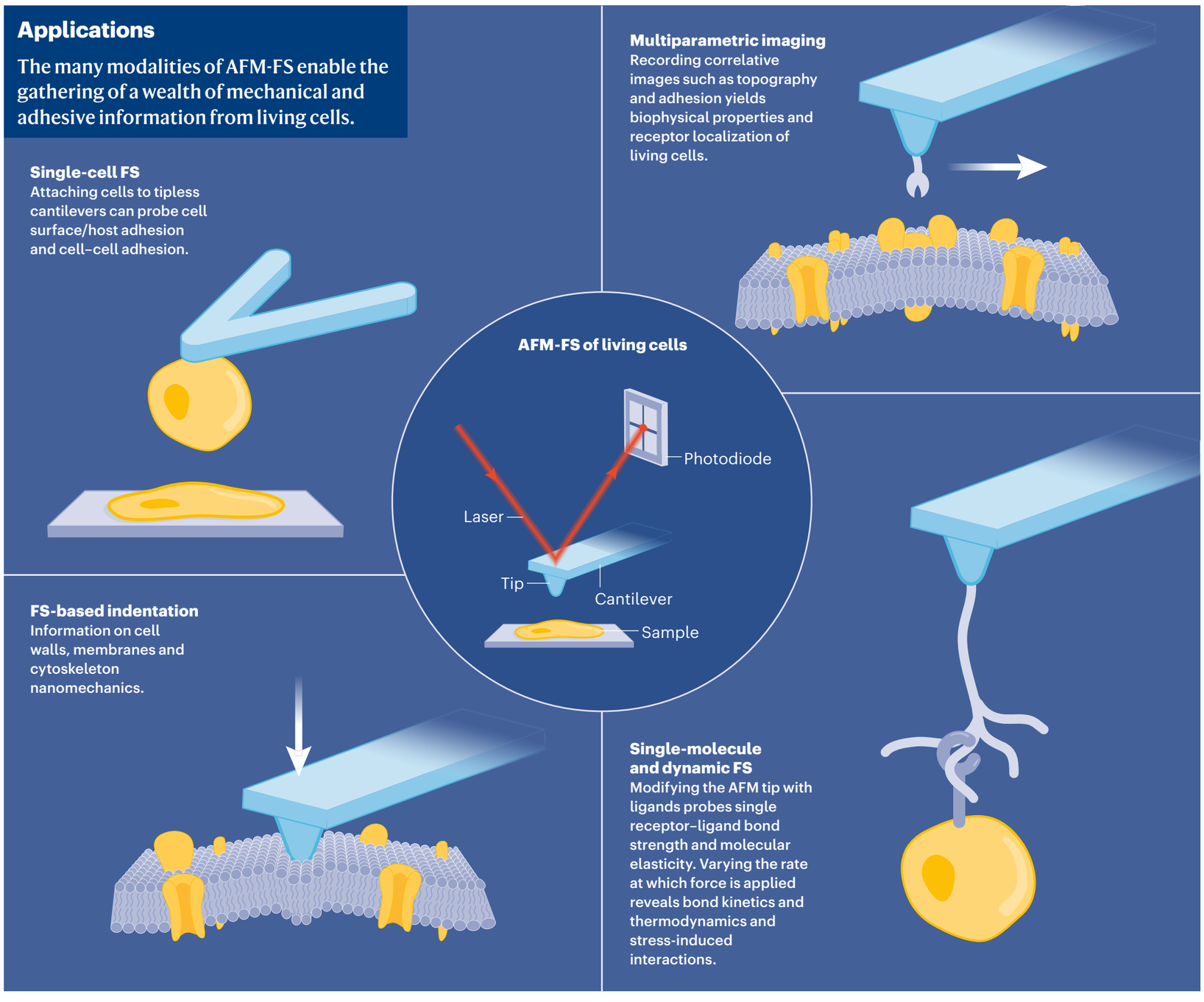

Reproducibility and data deposition

For statistics and reproducibility, hundreds of force–distance curves should be collected using more than ten cells and representative examples of retraction profiles should be shown. Data sets should be made publicly available and include experimental conditions (such as applied force and speed) and set-up configurations (such as cantilever properties). Microbial or animal cells must be immobilized on an appropriate substrate using non-destructive protocols to resist the forces exerted by the cantilever tip. It is also essential to demonstrate the specificity of targeted interactions when determining cell adhesion signatures.

Limitations and optimizations

Correct cantilever calibration is essential, and cantilever stiffness should preferentially match that of the cell. Typically, best results are obtained using cantilevers with small spring constants and short lengths because they exhibit low force noise. Each theoretical model applied to fit the data has advantages, limitations and specific assumptions that should be appropriately weighed to adequately choose the best model. Non-specific interactions can be minimized via a clean substrate and careful sample preparation.

Outlook

Although AFM-FS is a powerful platform to study cell adhesion and mechanics at the single-cell and single-molecule level, it has relatively low temporal resolution and only addresses the outer surface of cells. New tools combining AFM-FS with super-resolution microscopy, which probes the localization and motion of single molecules both outside and inside cells, will allow the identification of specific cellular components while simultaneously probing their properties and interactions.

Written by Kristina Maria Kareh; designed by Sam Whitham